| AD NUMBER |
|---|
| AD365696 |
| CLASSIFICATION CHANGES |

| TO: | UNCLASSIFIED |
|---|---|
| FROM: | CONFIDENTIAL |

| LIMITATION CHANGES |
|---|

TO:
Approved for public release; distribution is unlimited.

FROM:
Distribution authorized to U.S. Gov't. agencies and their contractors; Administrative/Operational Use; AUG 1965. Other requests shall be referred to Office of Naval Research, One Liberty Center, 875 North Randolph Street, Arlington, VA 22203-2114.

| AUTHORITY |
|---|

ONR ltr dtd 4 May 1977; ONR ltr dtd 4 May 1977

UNCLASSIFIED

| AD NUMBER |
|---|
| **AD365696** |
| CLASSIFICATION CHANGES |

TO:

CONFIDENTIAL

FROM:

SECRET

| AUTHORITY |
|---|
| 31 Aug 1968, Group 4, DoDD 5200.10 |

THIS PAGE IS UNCLASSIFIED

# SECURITY
# MARKING

The classified or limited status of this report applies
to each page, unless otherwise marked.
Separate page printouts MUST be marked accordingly.

SECRET

155687

(Unclassified Title)

# INVESTIGATION OF CONTROLLED PULSE LASER TECHNIQUES

FINAL TECHNICAL REPORT
August 1965

Advanced Research Projects Agency
Project Code 2730

Prepared under Contract Nonr 3920(00)
Annex C
by the Hughes Aircraft Company
Culver City, California

SECRET

155687

(Unclassified Title)

## INVESTIGATION OF CONTROLLED PULSE LASER TECHNIQUES

FINAL TECHNICAL REPORT
August 1965

ARPA Order Number 306-62
Project Code 2730

AUTHORS:

R. S. Congleton, Project Scientist
D. R. Dewhirst
A. W. Hatch
L. D. Riley

SDN 5-61043/27

Total Secret Pages: 43

# CONTENTS

## ILLUSTRATIONS

## I. INTRODUCTION AND SUMMARY

This report contains a technical summary of the work accomplished on Contract Nonr 3920(00), Annex C, during the period 1 March 1964 to 28 May 1965. A complete technical summary report (HAC Report No. P64-24, "Controlled-Pulse Laser and Ruby Storage Mode Investigation," April 1964) has been previously submitted on the work conducted on the basic contract including Annex A and Annex B.

The major achievements accomplished during work on Annex C are the following:

1. Development of an improved controlled pulse laser oscillator which does not require an external optical feedback loop.
2. Design, construction, and test of a controlled pulse laser oscillator-amplifier device which yielded energy output up to 30 joules in an 8-microsecond pulse.
3. Based upon the low energy controlled pulse laser oscillator-amplifier device design and test results, a design was completed for a high energy (in excess of 600-joule output) controlled pulse laser oscillator-amplifier device.

During the early portion of this program, a re-evaluation of methods of constructing a controled pulse oscillator was conducted to determine if a simpler and more efficient method could be developed to obtain controlled pulse laser emission. This re-evaluation resulted in the development of a controlled pulse laser oscillator which had some definite advantages over the designs previously used (see HAC Report No. P64-24, "Controlled-Pulse Laser and Ruby Storage Mode Investigation", April 1964). The external optical feedback loop was eliminated; an optical isolator was no longer required in the oscillator; and in addition, more efficient utilization of stored energy was obtained. These advantages have the effect of partially easing the requirements on the quality of the ruby. The analysis of the servo system used to obtain controlled pulse laser emission from this new oscillator design proved that the system could be made stable provided the optical and electrical delay times were appropriately adjusted. Several versions of the improved controlled

1

pulse laser oscillator were constructed and tested. These will be discussed in detail in a subsequent section. One disadvantage of the improved controlled pulse oscillator was that the design placed a more severe requirement on the transmission of the optical shutter, in this case a Kerr cell. An investigation of Kerr cell shutters resulted in a satisfactory solution to this problem.

The improved design of controlled pulse oscillator was incorporated into an oscillator-amplifier device to obtain higher energy output and to verify the feasibility of such a device. In order to reduce superfluorescence effects due to high gain, both an optical shutter and an optical isolator were incorporated into the device between the oscillator and amplifier. The optical shutter was closed during the pumping period and opened at the initiation of the controlled pulse laser sequence. Servo analysis and subsequent test of this device indicated that stable controlled pulse laser emission could be obtained by proper adjustment of optical and electrical delay times and gains.

Based upon the low energy controlled pulse laser oscillator-amplifier design and test results, a design for a higher energy device was evolved by scaling up from the lower energy device. Whereas the lower energy device used a single ruby crystal 14.5 millimeters in diameter by 8 inches long in both the oscillator and the amplifier, the proposed high energy design uses two similar laser crystals in parallel in the oscillator and 14 laser crystals in parallel in the amplifier. Since the gains, delay times, and servo system for the two devices are very nearly identical, the only expected difference in the performance would be increased energy due to parallel operation of the laser crystals.

2

## II. CONTROLLED PULSE LASER
## OPTICAL CONFIGURATIONS

### A. IMPROVED CONTROLLED PULSE LASER OSCILLATOR

Several configurations of controlled pulse laser oscillators are described in a previous report (HAC Report No. P64-24, April 1964). During the early portion of this program, an improved configuration for a controlled pulse laser oscillator was developed. In addition to eliminating the external optical feedback loop and optical isolator previously required, the new configuration provides a means of output coupling and feedback control which is more efficient than previous controlled pulse laser devices. Several variations of the improved controlled pulse oscillator have been constructed and operated successfully.

The optical layout of the oscillator is shown in Figure 1. It consists of five basic elements which are:

1.  Two multilayer dielectric reflectors (R = 100 percent nominal)
2.  Kerr cell[1]
3.  Wollaston prism
4.  Ruby and pumping cavity
5.  Servo control circuitry

The multilayer dielectric reflectors are aligned optically parallel for vertically polarized light (light polarized perpendicular to the paper). Vertically polarized laser radiation reflects back and forth between the reflectors passing through the ruby, Wollaston prism, and Kerr cell. The Kerr cell and Wollaston prism are the optical shutter and serve for both the feedback control and output coupling functions.

The optical shutter as shown in Figure 1 operates in the following manner: The Kerr cell is oriented with the electric field 45 degrees with respect to the vertical. Also the Wollaston prism and multilayer dielectric reflectors are aligned such that the optical cavity is resonant for vertically polarized light. Horizontally polarized light is then

3

deviated from the resonant optical path in passing through the Wollaston prism from either direction. Vertically polarized laser radiation from the ruby incident on the Wollaston prism from the right is reflected back on itself through the Kerr cell - Wollaston prism shutter. In passing twice through the Kerr cell, the laser radiation emerges elliptically polarized. The degree of elliptical polarization is a function of the Kerr cell voltage. The horizontally polarized component of the elliptically polarized light is the output beam and is deviated from the resonant optical path in passing from left to right through the Wollaston prism. The vertically polarized component remains in the resonant optical path as optical feedback.

During the pumping phase, the oscillator is prevented from lasering by applying quarter-wave voltage to the Kerr cell. For this voltage, light initially vertically polarized emerges from the Kerr cell horizontally polarized and is totally deviated from the resonant cavity. Since there is no feedback, laser oscillation is suppressed. To initiate the output pulse, the Kerr cell voltage is reduced from quarter-wave to allow feedback.

The Kerr cell voltage is controlled throughout the output pulse to adjust the feedback to the proper value to maintain the desired output power level. This is accomplished by reflecting a portion of the output beam into a servo photodiode which monitors the output beam power level and provides a correction voltage to the Kerr cell. A decrease of the output power level causes a voltage correction which increases the feedback, resulting in increased laser action and a concurrent rise in output power. Conversely, an increase of the output power level causes the feedback to be reduced. A more detailed discussion of the control function is given in a separate section.

A variation of the preceding controlled pulse laser is shown in Figure 2. In this oscillator, the locations of the ruby and Wollaston prism are interchanged. This results in some differences between the two oscillators, but basically they are the same.

The oscillator as shown in Figure 2 is aligned to be optically resonant for the vertical polarization (perpendicular to the paper).

4
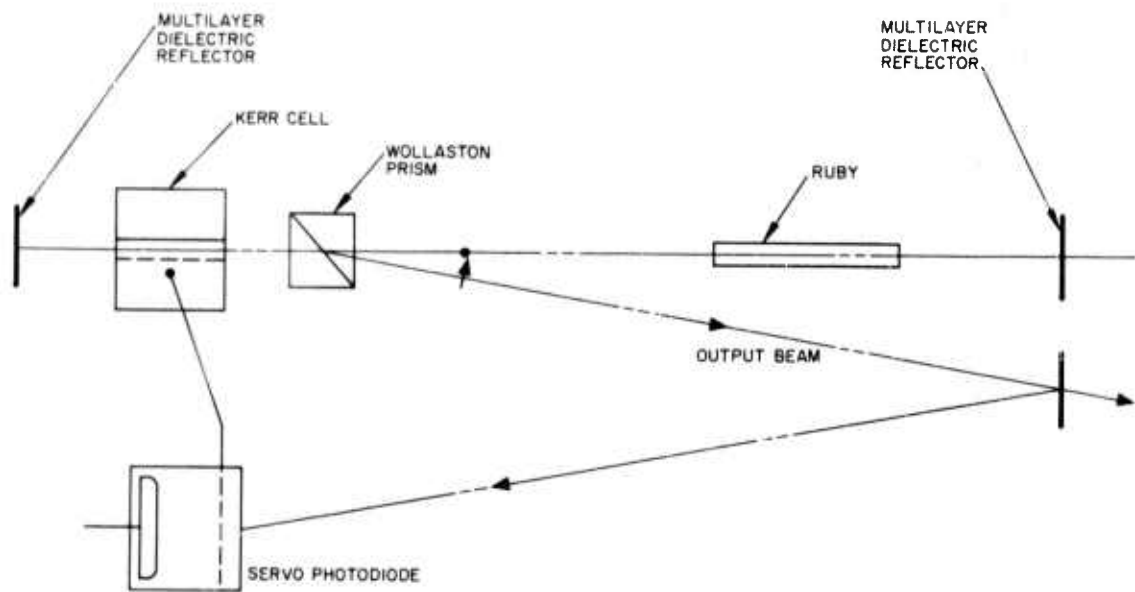
Figure 1. Improved controlled pulse laser oscillator, variation No. 1.
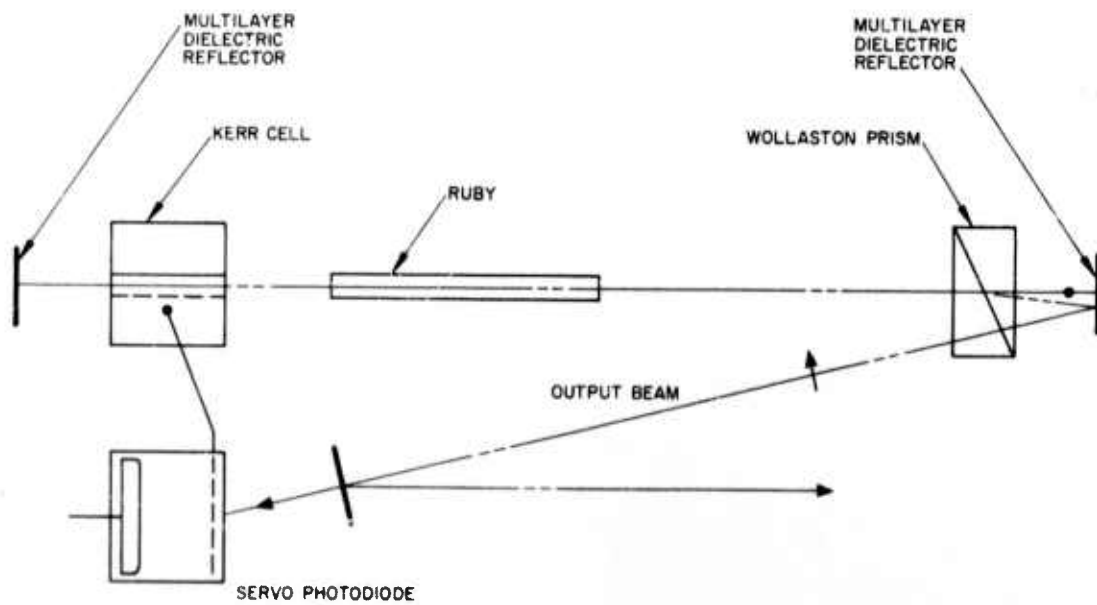


Figure 2. Improved controlled pulse laser oscillator, variation No. 2.

The operation of the Kerr cell-Wollaston prism shutter is identical to that described for Figure 1. Vertically polarized laser radiation incident on the Kerr cell from the right is elliptically polarized in passing twice through the Kerr cell. The component polarized vertically is the feedback and remains in the oscillator and the component polarized horizontally is deviated from the resonant optical path in passing through the Wollaston prism.

The oscillator arrangement shown in Figure 2 results in two major differences in operation. (1) The output beam is amplified in passing through the ruby before being deviated from the resonant cavity. (2) The output beam passes through the Wollaston prism twice before leaving the oscillator. This causes a doubling of the angle of separation between the output beam and resonant optical path.

A third variation of the new controlled pulse oscillator is shown in Figure 3. This oscillator is very similar to the first one described except a quarter-wave plate is added. The major advantage of this innovation is the Kerr cell is operated with zero voltage bias during the pumping phase.
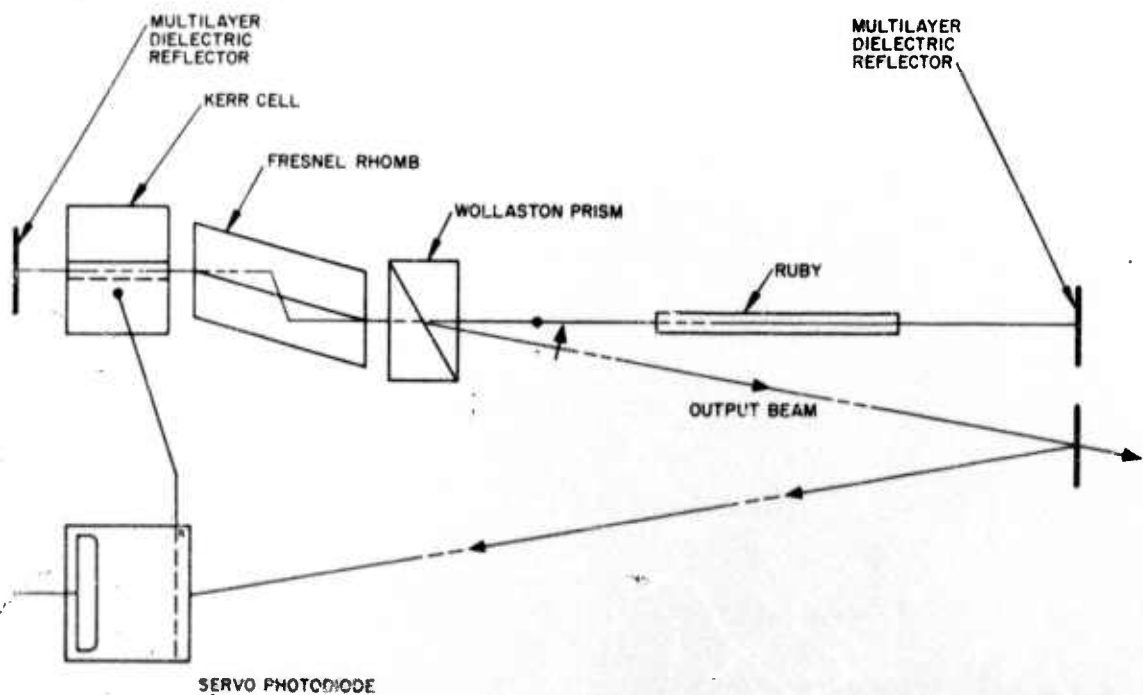
Figure 3. Improved controlled pulse laser oscillator, variation No. 3.

6

A major problem in the operation of the two oscillators described previously results from the fact that quarter-wave voltage is applied to the Kerr cell to prevent laser oscillation during the pumping phase. A characteristic of Kerr cells of typical quality is their tendency to develop an electric field gradient between the plates after voltage has been applied for some time. This degrades the uniformity of the null transmission of the Kerr cell - Wollaston prism shutter across the aperture and increases the minimum obtainable transmission at the null voltage. This effect is a limiting factor in the maximum gain to which the ruby crystal can be raised during the pumping period, since regeneration will occur as soon as unity gain is achieved in the regenerative cavity.

A second difficulty encountered in the operation of the two previous oscillators is the necessity of maintaining the exact Kerr cell bias voltage required for null transmission during the pumping period. For high gain rubies, the tolerance on this bias voltage is of the order of a few tens of volts in a net bias of tens of thousands of volts.

The addition of the quarter-wave plate in the regenerative cavity eliminates these difficulties. With the quarter-wave plate, the Kerr cell is operated at zero voltage during the pumping phase resulting in a much lower value for the minimum obtainable transmission through the shutter. The use of Kerr cells of only average quality operated with no critical high voltage bias is permitted even when the ruby is pumped to a very high gain condition.

The optical layout of the oscillator using a quarter-wave plate is shown in Figure 3. The quarter-wave plate is a Fresnel rhomb designed to give the quarter-wave phase retardation at the ruby laser wavelength. A detailed discussion of the Fresnel rhomb as a quarter-wave plate is given in Appendix A.

The optical operation of this device is identical to that shown in Figure 1 except the combination of the quarter-wave plate and Kerr cell performs the same function as the Kerr cell alone in the previous device. The quarter-wave plate provides an "optical bias" such that the shutter transmission is changed from a minimum at zero Kerr cell

7

voltage to a maximum at quarter-wave voltage. To initiate laser oscillation, voltage is applied to the Kerr cell to allow the required feedback. The voltage is then increased throughout the pulse to compensate for the decreasing ruby gain so that unity gain is maintained in the optical cavity.

The improved type of controlled pulse lasers described above offers several advantages over previous devices of this type. Some of these advantages are:

1. Smaller
2. Simpler to construct
3. More efficient utilization of stored energy
4. Shorter optical path
5. Requires lower Kerr cell voltage and voltage changes
6. Higher servo gain is achievable
7. Does not require an optical isolator.

E. KERR CELL - WOLLASTON PRISM SHUTTER

As described above, a major problem with Kerr cell-Wollaston prism shutters when high voltage has been applied for some time is the degradation of the null transmission caused by the electric field gradient. For Kerr cells of average quality, the null transmission is limited to about -15 db by this effect.

The electric field gradient is caused by a space charge which gradually develops between the plates when voltage is applied. The minimum single pass transmission through a Kerr cell - Wollaston prism shutter is obtained when the electric field between the plates is sufficient to cause a half-wave phase retardation between the components polarized parallel and perpendicular to the Kerr cell plates. However, when the electric field gradient has developed between the plates (i.e., the electric field varies in magnitude across the distance between the plates), it is impossible to obtain uniformly low transmission across the full aperture of the Kerr cell.

8

This effect is evident in the photographs of Figure 4. These were taken of the transmission of a 0.8 inch diameter gas laser beam (6328 Å) through the Kerr cell-Wollaston prism combination. The region of extinction is the dark band running vertically through the beam cross section. It is evident from these photographs, taken at different Kerr cell voltages, that the position of this band varies according to the applied voltage.

The problem caused by the electric field gradient can be avoided by suddenly applying voltage to the Kerr cell at the start of the desired shutter off time as opposed to applying it for a long period of time before the desired off time. When this is done, the space charge from which the electric field gradient results does not have sufficient time to develop during the desired shutter off time. The application of voltage for a long period of time prior to the desired off time is in most instances a matter of convenience and not necessity.

Transmission measurements were made with null voltage on a Kerr cell-Wollaston prism shutter of typical quality. These were made after voltage was applied for a sufficient time to allow the electric field gradient to develop. Figure 5 shows the results of these measurements on a logarithmic scale. The Kerr cell used has a 0.8-inch plate separation and a half-wave voltage of about 34 kv.

The transmission through the shutter was measured in seven positions across the distance between the Kerr cell plates with a 0.2-inch diameter gas laser beam operating at 6328 Å. In taking the measurements, the voltage was first adjusted to obtain minimum transmission through the center of the Kerr cell. As is shown in the figure, the transmission varied considerably across the Kerr cell aperture.

The transmissions measured for each beam position are actually averages over the gas laser beam cross-section. For this reason, the null transmission through the exact center of the Kerr cell was probably lower than that shown. It was also noted that by varying the voltage, the transmission anywhere between the Kerr cell plates would be made as low as about -20 db. Any single voltage could not, however, give uniformly low transmission across the full aperture due to the non-uniformity of the electric field (see Figure 4).

9

ANOOE

CATHODE

ANOOE

CATHOOE

36 KV

33 KV

35 KV

32 KV

34 KV

3I KV
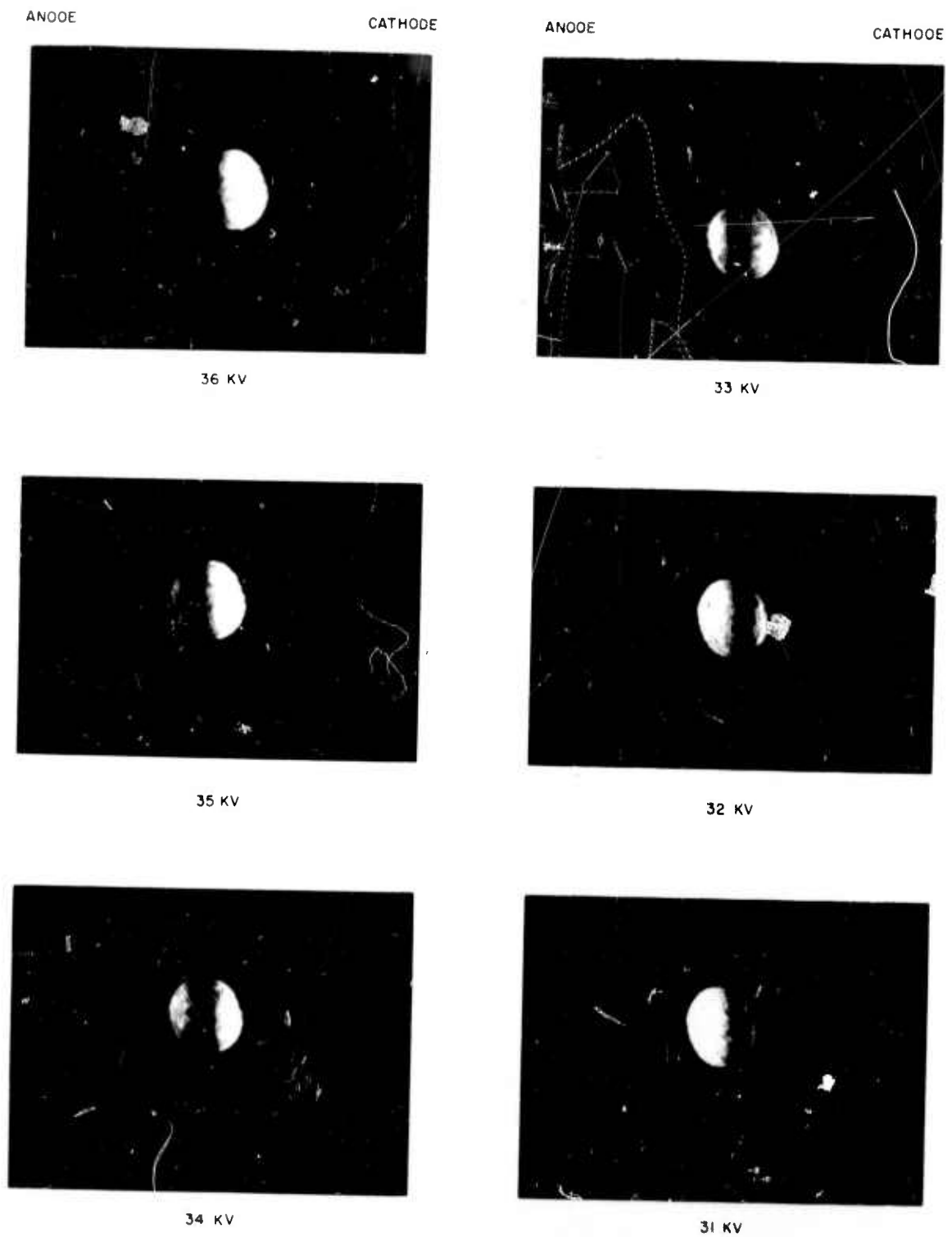
Figure 4.   Transmission through a Kerr cell -Wollaston prism shutter.

10
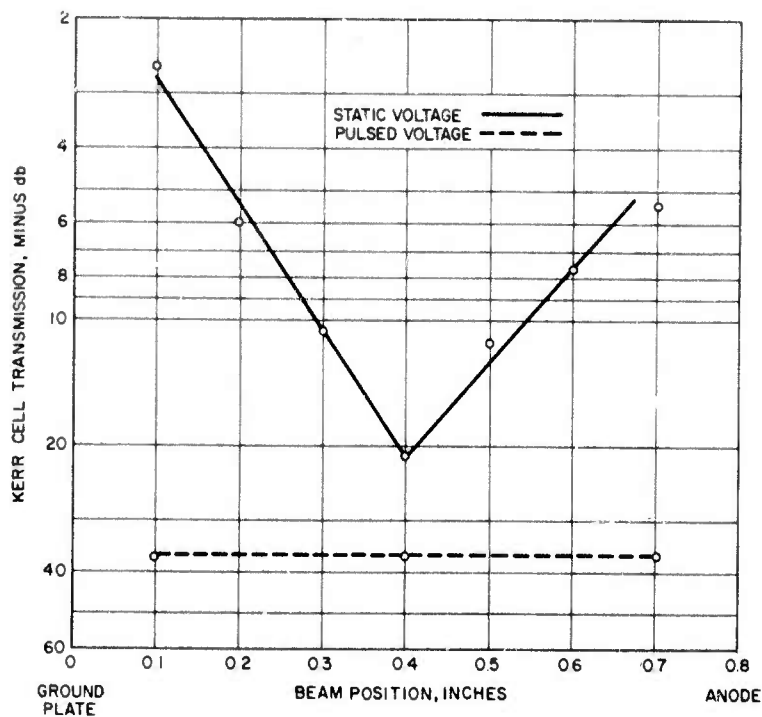
Figure 5. Static and pulsed transmission through
Kerr cell-Wollaston prism shutter.

Using the same Kerr cell, the null transmission was also
measured for the case in which the voltage was suddenly applied. A
circuit to accomplish the sudden application of voltage to the Kerr cell
is shown in Figure 6. Since it would be difficult to build up voltage on
one plate rapidly, half-wave voltage was gradually applied to both
plates some time before the desired shutter off time. One plate was
then suddenly connected to ground by the thyratron leaving half-wave
voltage between the plates. During the time voltage is being applied to
both plates, the voltage drop across the plates is zero, thereby pre-
venting the space charge occurrance.

By suddenly applying half-wave voltage in the manner described
above, the transmission through the Kerr cell - Wollaston prism
shutter was measured to be minus 36 db. Furthermore, it was uniform
across the entire Kerr cell aperture to within one-half db. This com-
pares quite favorably with the transmission curve shown in Figure 5 using
the same Kerr cell. Figure 7 summarizes the results of static and
pulsed operations.

11
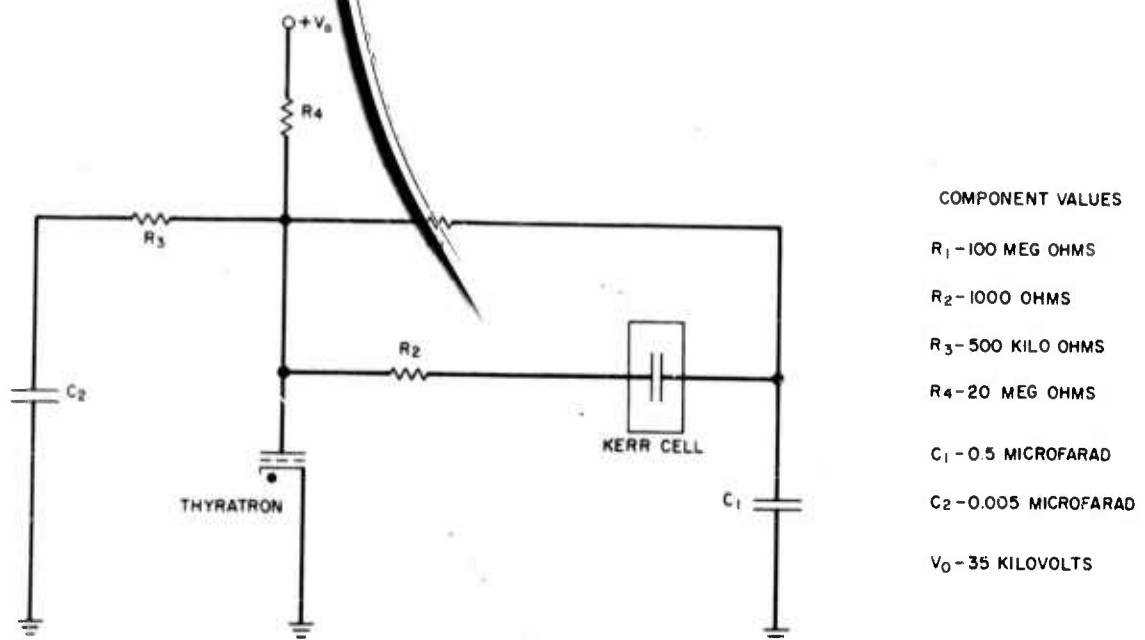
Figure 6. Kerr cell - Wollaston prism switch circuit.

COMPONENT VALUES

$R_1$ - 100 MEG OHMS

$R_2$ - 1000 OHMS

$R_3$ - 500 KILO OHMS

$R_4$ - 20 MEG OHMS

$C_1$ - 0.5 MICROFARAD

$C_2$ - 0.005 MICROFARAD

$V_0$ - 35 KILOVOLTS

| CONDITIONS | WIDE BEAM, 0.8 IN. DIA | NARROW BEAM, 0.2 IN. DIA |
|---|---|---|
| WOLLASTONS CROSSED KERR CELL OFF | -47.0 db | -48.0 db |
| WOLLASTONS ALIGNED KERR CELL ON, 34 KV STATIC CASE | -14.3 db | -21.0 db |
| WOLLASTONS ALIGNED KERR CELL PULSED ON 34 KV | -38.7 db | -36.4 db |

Figure 7. Summary of Kerr cell transmission data.

## C. CONTROLLED PULSE OSCILLATOR-AMPLIFIER DEVICE

In an effort to realize a greater amount of energy output from the controlled pulse laser, a combination oscillator-amplifier device was constructed (Figure 8). The oscillator for this device is the one described previously using a Fresnel rhomb quarter-wave plate.
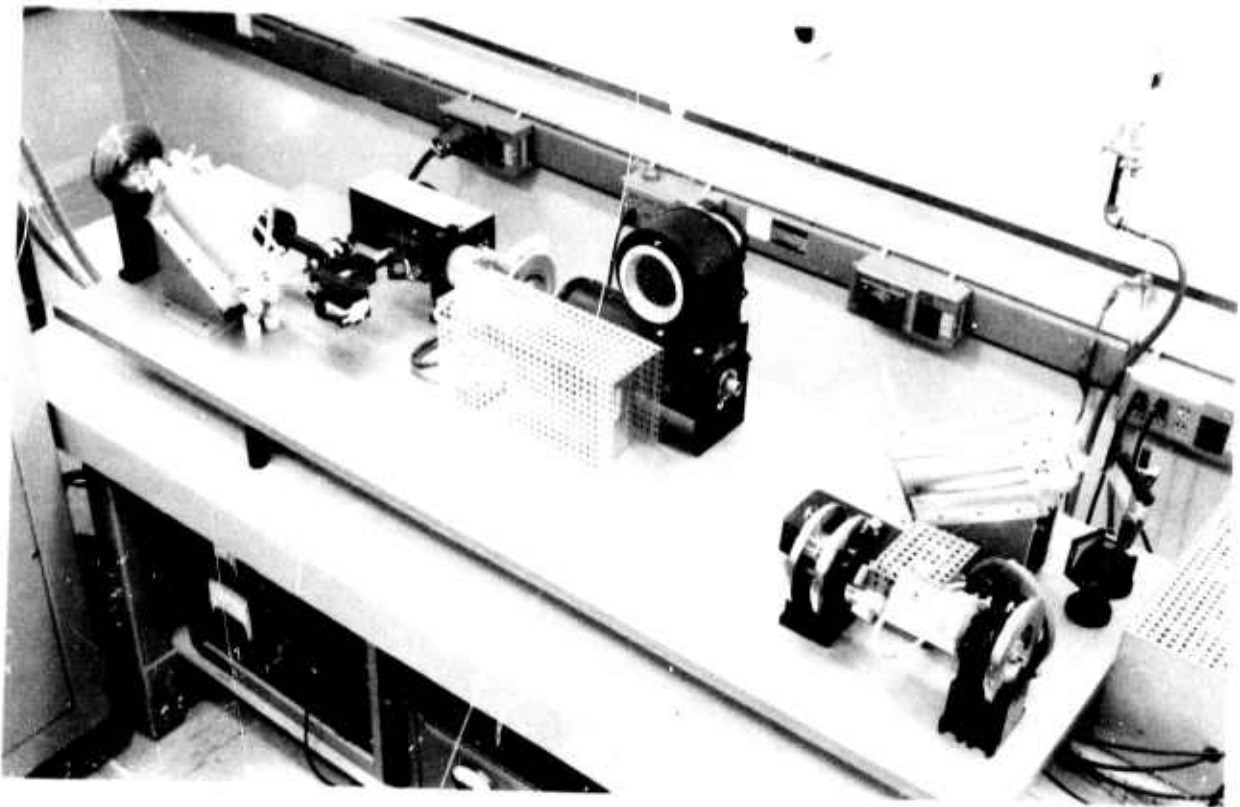


Figure 8. Oscillator-amplifier device.

A notable feature of this device is the use of an optical switch and optical isolator between the oscillator and amplifier. Their purpose is to prevent undesirable coupling between oscillator and amplifier which would tend to depump the amplifier ruby. The use of the switch and isolator allows the amplifier ruby to be pumped to a much higher gain than would be otherwise possible.

The optical configuration of the oscillator-amplifier is illustrated in Figure 9. The oscillator cavity is aligned to be regenerative for the vertical polarization when voltage is applied to the control Kerr cell. The horizontally polarized output radiation from the oscillator is

13
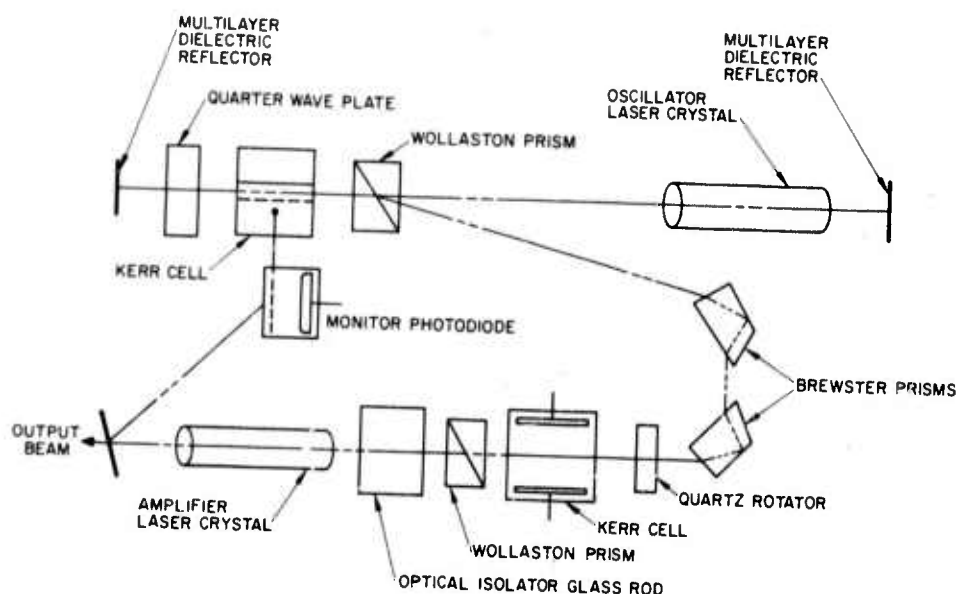
Figure 9. Controlled pulse laser oscillator-amplifier optical layout.

directed into the amplifier path by two prisms. The entrance and exit windows of these are at Brewster's angle for the purpose of minimizing the reflection loss.

Before passing through the amplifier, the oscillator output first goes through a Kerr cell switch and an optical isolator. The components of the switch are the Kerr cell and Wollaston prism and those of the isolator are the quartz rotator, the Wollaston prism, and dense flint glass rod. The Wollaston prism is common to both the switch and isolator. The function of the switch is to decouple the oscillator and amplifier during the pumping phase. It is pulsed on at the start of the output pulse. The isolator prevents spontaneous emission originating in the amplifier from reaching the oscillator during both the pumping phase and output pulse.

The oscillator output experiences the following in traversing the path to the amplifier. In passing through the quartz rotator, the polarization vector of the incident radiation is rotated 45 degrees in a clockwise direction as seen by an observer facing the direction of propagation. The laser radiation next passes through a Kerr cell to which half-wave voltage is applied during the output pulse.

14

Since the plates of the Kerr cell are in the vertical plane, the Kerr cell birefringence at half-wave voltage effectively rotates the polarization vector of the laser radiation by an additional 90 degrees. The emerging radiation is therefore polarized at a 45 degree angle counter-clockwise from the vertical as seen by an observer facing the direction of propagation. The Wollaston prism is aligned so as to direct this polarization into the amplifier crystal, while deflecting the orthogonally polarized component. Therefore, the horizontally polarized output of the oscillator is not coupled into the amplifier until half-wave voltage is applied to the Kerr cell. Since there is zero electric field within the Kerr cell during the pumping period, Kerr cell quality is not a limiting factor in achieving maximum decoupling.

The dense flint glass rod of the optical isolator is located between the Wollaston prism and laser amplifier. The theory and construction of the optical isolator have been described elsewhere. The isolator rod rotates the polarization vector of the laser radiation by 45 degrees clockwise as seen by an observer facing the direction of propagation. The laser radiation which enters the amplifier is therefore vertically polarized.

The output of the amplifier is sampled by a beam splitter which deflects a small portion of the radiation into a high current, high speed monitor photodiode. This device is coupled to the oscillator Kerr cell, thereby providing servomechanism control of the oscillator regeneration.

An important feature of the device is its ability to suppress spurious regeneration between oscillator and amplifier rubies both during the pumping phase and output pulse. This feature allows the oscillator and amplifier rubies to be pumped to much higher gains than would be otherwise possible, resulting in greater energy extraction from the rubies.

The depumping suppression is accomplished by the use of the Kerr cell switch and optical isolator described previously. In the absence of these components, there exists two paths of coupling between the oscillator and amplifier, both of which would tend to depump the output end of the amplifier ruby. The net effect of this depumping would be that it would be impossible to pump the output end of the amplifier to a high level of inversion.

15

Consider in Figure 10 vertically polarized spontaneous emission originating at point 1 in the oscillator ruby and travelling the path 1-2-3-4-5-4-6-7-8-9. In travelling this path, the spontaneous emission undergoes twice the oscillator gain plus the amplifier gain. In a fully pumped condition, the oscillator gain is about 20 db and the amplifier gain 25 db, resulting in a total of about 65 db for a fully pumped condition. In comparing this gain with the rate of spontaneous emission and the solid angle subtended by the amplifier output aperture at point 1 along the depumping path, it is found that the depumping from this path is not significant during the time span of the output pulse, but would have an appreciable effect during the pump period. For this reason, the Kerr cell switch is inserted to decouple the oscillator and amplifier during the pumping time.
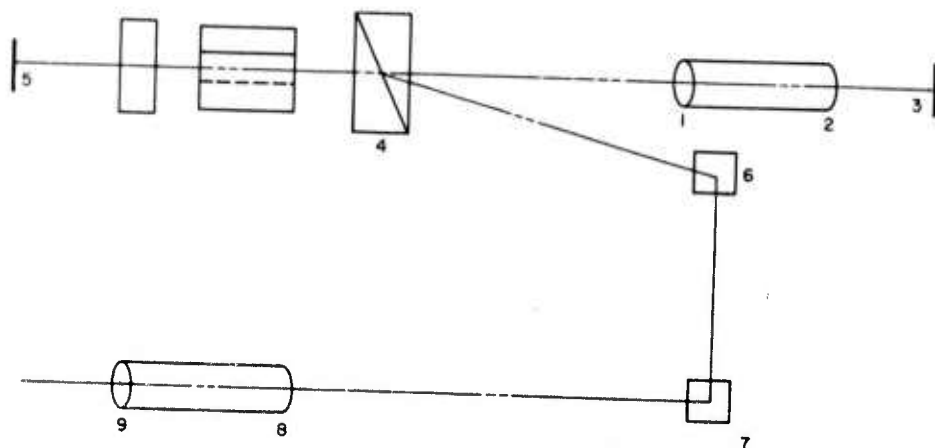


Figure 10. Depumping paths.

The second path is even more effective in depumping the output end of the amplifier. This is for vertically polarized spontaneous emission originating in the output end of the amplifier and travelling the path 9-8-7-6-4-5-4-1-2-3-4-5-4-6-7-8-9. The gain for this path is 90 db. This gain, when compared with the spontaneous emission rate and the solid angle for the path, is found to be sufficient to cause a significant effect even during the short time of the output pulse. For this reason, an isolator is included with the Kerr cell switch to prevent vertically polarized spontaneous emission from the amplifier from reaching the oscillator. The isolator is operative at all times during the pump period and output pulse. It may be noted here that during the

output pulse, the isolator and switch allow horizontally polarized light from the amplifier to reach the oscillator. However, since 60 degrees orientation rubies are used, the gain is not sufficient for this polarization to cause significant depumping during the output pulse.

17

### III. PULSE CONTROL

A. SERVO ANALYSIS:

Controlled-pulse operation of the new laser oscillators described above involves consideration of their inherent stability. Previous servo control studies had emphasized the determination and quantitative evaluation of a satisfactory servo control function for a given stable oscillator configuration. It was now desirable to analytically compare several different oscillators from the standpoint of transport delay effects on stability.

Accordingly, simplified and linearized equations governing the small-signal behavior of each controlled oscillator were developed. Translated into the frequency domain, these equations are processed to define a characteristic complex function for each oscillator configuration. Application of the Nyquist stability criterion to this function determines the effects on stability of various transport delays. Different oscillator configurations may therefore be evaluated by comparison of their characteristic functions.

While this rather conventional approach to the analytical problem becomes quite intractable for servo transfer functions more complex than a zero time constant fast servo with no integrator, the difficulty of obtaining easily variable transport delays of high bandwidth seems to preclude direct analog computer simulation of each oscillator.

The following will illustrate a method for obtaining the characteristic function of these devices. The laser oscillator chosen for this example is the first of those described in the previous section. An amplifier has been included in the system to maintain generality and to demonstrate that the small-signal characteristics of oscillator control are for all practical purposes unaffected by the inclusion of output amplification. A schematic of the oscillator-amplifier is shown in Figure 11.
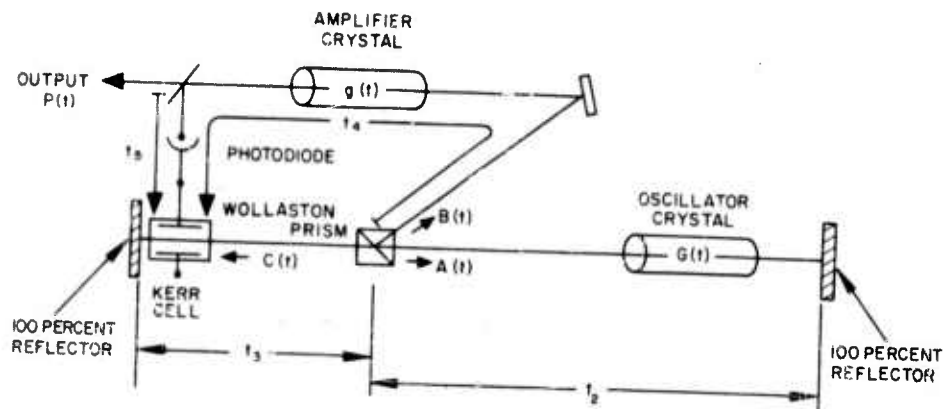
Figure 11. Controlled oscillator-amplifier schematic.

Definition of Symbols:

$t_2$, $t_3$, $t_4$, $t_5$ = optical and electronic transport delays as shown in Figure 11.

$A(t)$ = power fed back into oscillator regenerative cavity.

$B(t)$ = power ejected from oscillator regenerative cavity.

$C(t)$ = power incident on Kerr cell from oscillator crystal.

$P(t)$ = output power level of system as monitored at photodiode beamsplitter

$T(t)$ = "feedback transmission": the fraction of $C(t)$ which, after a delay of $t_3$, will appear as the ejected component "B". $T(t)$ is determined by the instantaneous Kerr cell voltage, which is the sum of the "program" and "servo" input voltages.

$G(t)$ = numerical power gain for a small signal passing once through the oscillator crystal.

$g(t)$ = numerical power gain for a small signal passing once through the amplifier crystal.

Since both the duration of the controlled pulse and the total stored energy to be extracted from the amplifier and oscillator crystals are known, the expected time behavior of both the small signal gain of each laser crystal and the power levels throughout the system may be computed. The required feedback transmission function is also easily computed. These computed functions may be denoted as $G_o(t)$, $g_o(t)$, $A_o(t)$,

20

$B_o(t)$, $C_o(t)$, and $T_o(t)$. The computed output power waveform $P(t)$ is the fixed level $P_o$ throughout the controlled pulse.

The present analysis is concerned with system operation over a time interval much shorter than the controlled pulse duration but much longer than any of the transport delays involved. During this interval, therefore, the amount of change of each of the computed time functions will be very small. The values of these functions during this period may be denoted by the "constants" $G_o$, $g_o$, $A_o$, $B_o$, $C_o$, and $T_o$, bearing in mind the variation of these values from one interval to another. From inspection of the system layout, then, during any given interval of observation the following "d-c" relationships must be satisfied:

$$A_o = T_o C_o$$
$$B_o = (1 - T_o) C_o$$
$$C_o = G_o^2 A_o$$
$$P_o = g_o B_o$$
$$T_o G_o^2 = 1$$

The last of these relationships is a consequence of the first and the third. It represents the "unity-gain" equilibrium of the idealized lossless regenerative oscillator.

The small-signal variations of the actual system waveforms from the computed values are thus defined during the period of interest as follows:

$$\Delta A(t) = A(t) - A_o$$
$$\Delta B(t) = B(t) - B_o$$
$$\Delta C(t) = C(t) - C_o$$
$$\Delta P(t) = P(t) - P_o$$
$$\Delta T(t) = T(t) - T_o$$

The actual power gain of each of the laser crystals will also exhibit small-signal deviations from the computed value $G_o$ or $g_o$ during

21

this time interval. These variations must depend on two factors: the history of the system prior to the interval of observation; and the integral of the deviations in the output power waveforms of the crystals during this interval. The first factor is eliminated by assuming the system to be in the computed equilibrium condition at the initiation of observation; the response of the system to known gain disturbances applied during the observation interval will be used to provide the desired information about its stability. The second factor is actually a stabilizing "integrating" influence since output power increases tend to lower the laser crystal gains from their computed values. The magnitude of this effect for small-signal power fluctuations has however been shown to be negligible during previous analog simulation.

Treating the laser crystal gains as fixed values, therefore, the time-domain equations governing operation of the system during the interval of interest are as follows:

$$A(t) = T(t - t_3) \cdot C(t - t_3)$$

$$B(t) = [1 - T(t - t_3)] \cdot C(t - t_3)$$

$$C(t) = G_o^2 \cdot A(t - <2t_2 + t_3>)$$

$$P(t) = g_o \cdot B(t - <t_4 - t_5>)$$

$$T(t) = T_o + \alpha(t) + (-HT_o/P_o) \cdot \Delta P(t - t_5)$$

Here the terminology $T(t - t_3)$, for example, denotes that the function $T(t)$ has been delayed by the transport delay $t_3$.

While the first four expressions follow at once from the system layout, the last equation involves some new definitions. The first two terms of this equation denote the programmed transmission function as it is actually applied to the Kerr cell; $\alpha(t)$, which by hypothesis is much less than $T_o$, represents any error in the programmed transmission. Since it is immaterial whether the unity-gain equilibrium of the oscillator regenerative cavity is disturbed by a shutter transmission error or by a laser gain fluctuation, $\alpha(t)$ may be used to represent both physical cases.

The last term of the equation for T(t) represents the corrective action of the servo. The symbol "H" denotes the overall real gain of the servo; here the imaginary part of the servo gain is assumed to be zero to facilitate the time-domain expression. The complex nature of the actual servo transfer function will be represented by $H(\Delta)$ in the frequency-domain equations. The quantitative definition of the real "servo gain" is as follows: "H" is equal to the percent step correction in feedback transmission, $\Delta T/T_0$, divided by the corresponding percent step disturbance $\Delta P/P_0$ which preceded the correction by the delay $t_5$. Typically, $0 < H < 2$ is the region of interest for these systems.

Substituting the small-signal terms in the above equations and dropping the "d-c" relationships, the following incremental equations are obtained:

$$\Delta A(t) = C_0 \cdot \Delta T(t - t_3) + T_0 \cdot \Delta C(t - t_3) + \Delta T(t - t_3) \cdot \Delta C(t - t_3)$$

$$\Delta B(t) = [1 - T_0] \cdot \Delta C(t - t_3) - C_0 \cdot \Delta T(t - t_3) - \Delta T(t - t_3) \cdot \Delta C(t - t_3)$$

$$\Delta C(t) = G_0^2 \cdot \Delta A(t - <2t_2 + t_3>)$$

$$\Delta P(t) = g_0 \cdot \Delta B(t - <t_4 - t_5>)$$

$$\Delta T(t) = \alpha(t) + (-HT_0/P_0) \cdot \Delta P(t - t_5)$$

The small-signal assumption justifies deletion of the incremental cross products in the first two equations since both $\Delta T$ and $\Delta C$ are small compared to $T_0$ and $C_0$ respectively. Translation of the resulting equations into the frequency domain or "$\Delta$-plane" yields the following:

$$\Delta A(\Delta) = C_0 \cdot \Delta T(\Delta) \cdot e^{-\Delta t_3} + T_0 \cdot \Delta C(\Delta) \cdot e^{-\Delta t_3}$$

$$\Delta B(\Delta) = [1 - T_0] \cdot \Delta C(\Delta) \cdot e^{-\Delta t_3} - C_0 \cdot \Delta T(\Delta) \cdot e^{-\Delta t_3}$$

$$\Delta C(\Delta) = G_0^2 \cdot \Delta A(\Delta) \cdot e^{-\Delta(2t_2 + t_3)}$$

$$\Delta P(\Delta) = g_0 \cdot \Delta B(\Delta) \cdot e^{-\Delta(t_4 - t_5)}$$

$$\Delta T(\Delta) = \alpha(\Delta) + (-T_0/P_0) \cdot H(\Delta) \cdot \Delta P(\Delta) \cdot e^{-\Delta t_5}$$

23

The exponential terms represent the Laplace transforms of the corresponding transport delays. These equations may be expressed in the form of a Signal Flow Graph, Figure 12.

A Signal Flow Graph[*] is useful in computing the response of any linear system to an applied input disturbance at some point in the system. In the present example, the disturbance could be an "error" in the programmed feedback transmission and the response would be measured as the corresponding change in output power. The transmission function which relates $\Delta P(\lambda)$ to $\alpha(\lambda)$ may be readily calculated from the above Signal Flow Graph. The important quantity, however, is not this expression itself but rather its denominator. It may be shown that the denominators of all transmission functions for a given flow graph are identical; this expression is referred to as the "determinant" of the Signal Flow Graph, and is in fact the "characteristic function" mentioned at the start of this example.

The graph determinant is easily evaluated as a function of the "loops" $L_1$, $L_2$, and $L_3$ indicated on the flow graph.[*]

$$\Delta(\lambda) = 1 - L_1 - L_2 - L_3 + L_1 L_3$$

$$= 1 - T_o G_o^2 e^{-\lambda(2t_2 + 2t_3)} + C_o G_o^2 (1 - T_o) g_o (T_o/P_o) \cdot H(\lambda) e^{-\lambda(2t_2 + 3t_3 + t_4)}$$

$$- C_o g_o (T_o/P_o) \cdot H(\lambda) e^{-\lambda(t_3 + t_4)} + T_o G_o^2 C_o g_o (T_o/P_o) \cdot H(\lambda) e^{-\lambda(2t_2 + 3t_3 + t_4)}$$

Eliminating the constants through their identities and simplifying, the following final result is obtained:

$$\Delta(\lambda) = 1 - e^{-\lambda(2t_2 + 2t_3)} + [1/(1 - T_o)] \cdot H(\lambda) e^{-\lambda(2t_2 + 3t_3 + t_4)}$$

$$- [T_o/(1 - T_o)] \cdot H(\lambda) e^{-\lambda(t_3 + t_4)}$$

---

[*]Mason, S.J., Electronic Circuits, Signals, and Systems, New York: John Wiley and Sons, 1960.
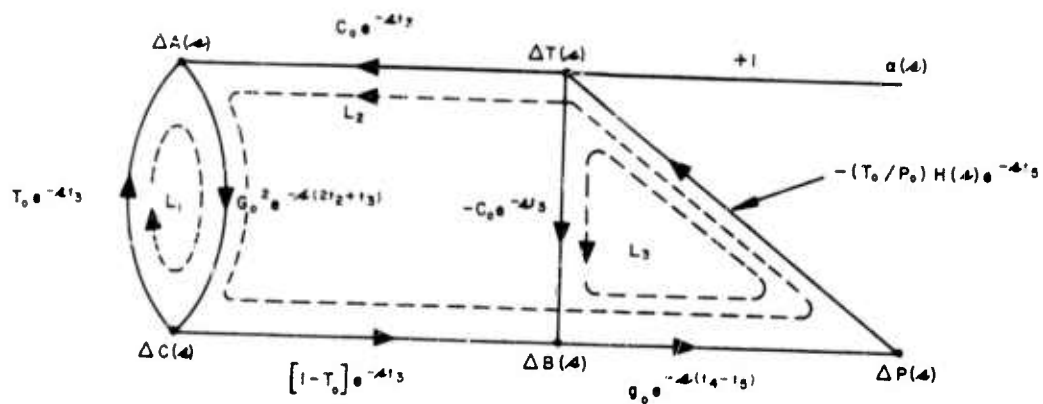
Figure 12. Signal flow graph.

Physically, the first term of $\Delta(\lambda)$ may be associated with the unity-gain regenerative oscillator loop itself; the time required for a complete round trip around this cavity is $(2t_2 + 2t_3)$. The second term represents the corrective action of the servo itself; note that any applied gain or power disturbance is not positively corrected until after a transport delay of $(2t_2 + 3t_3 + t_4)$. The third term represents the wrong-polarity correction which appears after a delay of $(t_3 + t_4)$ from the applied disturbance $\alpha(t)$. Fortunately, since $T_o$ is generally much less than unity, the effect of this unstable influence is very small.

Note that the time-variant nature of this system over the duration of the output pulse is reflected in the characteristic function by the inclusion of the computed feedback transmission $T_o$, which exhibits such long-term variation as described above. Alternatively, of course, $T_o$ could be replaced by $1/G_o^2$ or $A_o/C_o$. Note that the amplifier gain $g_o$ does not appear implicitly in this function, however.

The graph determinant $\Delta(\lambda)$ contains the desired stability information about the system. The zeroes of $\Delta(\lambda)$ must represent poles of the system transmissions since $\Delta(\lambda)$ is the denominator of each of these functions and since the numerators of the various transmission functions are composed of sums of products of stable functions. A conventional Nyquist approach is one method which may be used to evaluate the stability of the system, subject to the limitations and approximations which have been outlined in the course of the preceding example.

Before presenting some results of the application of the Nyquist analysis to the controlled-pulse laser problem, it will be illuminating

25

to compare the characteristic functions or graph determinants for several oscillator configurations which have been considered or constructed during the course of the present contract. These systems, together with the corresponding expressions for $\Delta(\lambda)$, are presented in Figure 13.

Oscillator configurations I and II are representative of the devices described in the foregoing section of this report. Since the determinants of their flow graphs are identical, their stability characteristics must also be identical within the small-signal region of validity of this analysis.

Some unidirectional regenerative oscillators considered previously are presented as configurations III, IV, and V for purposes of comparison. Inspection of its determinant shows that III is actually very similar in control performance to I and II. The major difference is that $T_o$ will be greater in III for a given laser crystal gain $G_o$ since each regenerative cycle involves only one pass through the crystal instead of two. Hence the detrimental factor associated with the last term of $\Delta(\lambda)$ will be more influential in oscillator III than in I or II.

Systems IV and V are seen to be identical from the standpoint of their graph determinants; the basic control difference between these systems is that in V we may set $t_2 \geq t_4$ quite conveniently, at a price of reduced overall efficiency as compared with IV. These two systems are capable of time-invariant performance throughout the duration of the controlled pulse since the expression for their determinants is independent of the time-variant factor $T_o$. Systems IV and V will not, however, be free of time variation in their control behavior if only one Kerr cell is used for both the program and servo functions, since the magnitude of $H(\lambda)$ will be a function of the varying Kerr cell sensitivity. Finally, the unstable "wrong polarity" correction term common to the graph determinants for the first three configurations does not appear in IV or V.

The basic similarity of the determinants of these oscillators suggests that a common Nyquist analysis of their stability characteristics could be made to yield information about all systems. The following approximation establishes the generalization: If $T_o \ll 1$ in systems I, II, and III, the last term in the expressions for $\Delta(\lambda)$ may be neglected and the coefficient of the preceding term may be set to unity. This approximation will lead to a somewhat optimistic stability evaluation which will
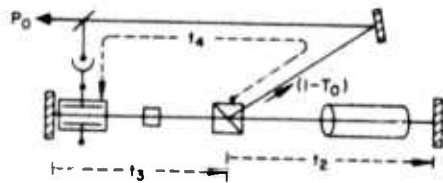
$$\Delta(\omega) = 1 - e^{-\omega(2t_3 + 2t_2)} + [1/(1-T_0)] H(\omega) e^{-\omega(2t_2 + 3t_3 + t_4)}$$
$$- [T_0/(1-T_0)] H(\omega) e^{-\omega(t_3 + t_4)}$$

CONFIGURATION I.

$$\Delta(\omega) = 1 - e^{-\omega(t_2 + t_3)} + H(\omega) e^{-\omega(t_2 + t_4)}$$
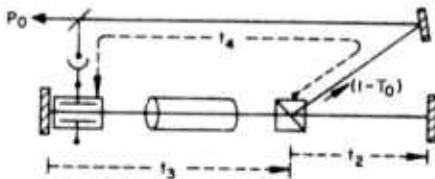
CONFIGURATION IV.

$$\Delta(\omega) = (\text{IDENTICAL TO } \Delta(\omega) \text{ FOR CONFIGURATION I.})$$

CONFIGURATION II.

$$\Delta(\omega) = 1 - e^{-\omega(t_2 + t_3)} + H(\omega) e^{-\omega(t_2 + t_4)}$$
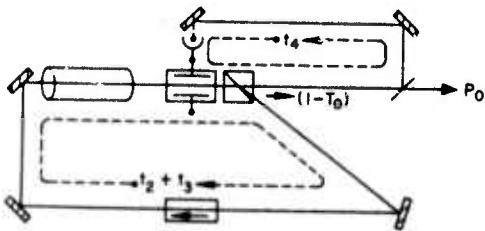
CONFIGURATION V.

$$\Delta(\omega) = 1 - e^{-\omega(t_2 + t_3)} + [1/(1-T_0)] H(\omega) e^{-\omega(t_2 + t_3 + t_4)}$$
$$- [T_0/(1-T_0)] H(\omega) e^{-\omega t_4}$$

CONFIGURATION III.

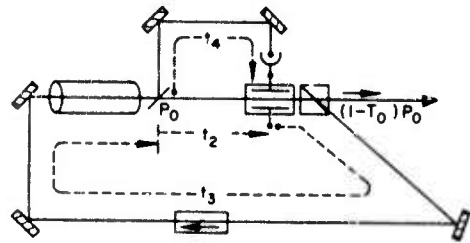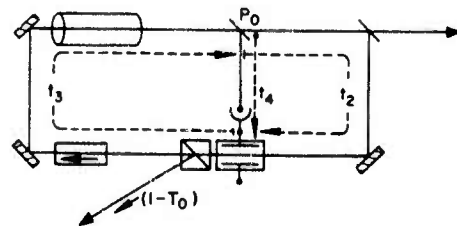KEY TO OPTICAL COMPONENTS:

| | | | |
|---|---|---|---|
| | LASER CRYSTAL | | SERVO PHOTODIODE |
| | KERR CELL | | 100% REFLECTOR |
| | WOLLASTON PRISM | | BEAMSPLITTER |
| | QUARTER-WAVE PLATE | | OPTICAL ISOLATOR |

Figure 13. Oscillator configurations.

be more accurate for typical operation of systems I and II than for III, since configurations I and II have $T_o = 0.01$ for $G_o = 10$, while system III requires $T_o = 0.10$ for $G_o = 10$.

With these considerations in mind, the expressions for $\Delta(\lambda)$ for all five oscillators may be reduced to the common expression:

$$\Delta(\lambda) = 1 - e^{-\lambda t_L} + H(\lambda) e^{-\lambda(t_L + t_d)}$$

The general transport delays $t_L$ and $t_d$ are defined as follows:

$t_L$ = total "round trip" transport delay in the regenerative cavity.

$t_d$ = difference between the total positive servo correction transport delay and $t_L$.

The imaginary part of $H(\lambda)$ may be set equal to zero for the initial Nyquist evaluation, thereby isolating the effects of the parameters $t_L$ and $t_d$. This analysis will determine the maximum allowable value of the gain H of the zero-time constant servo for various combinations of the parameters $t_L$ and $t_d$. In this manner a good indication of the relative intrinsic stability of the various oscillator configurations will be obtained since the restraints on the transport delays $t_L$ and $t_d$ differ from one device to another.

The results of this analysis are presented in Figure 14, where the parameter of interest is the ratio $t_d/t_L$. The maximum stable value of the real servo gain H is seen to be a nonzero value only for values of $t_d$ which are exact integral multiples of $t_L$: $t_d = nt_L$, where $-1 \leq n < \infty$. The value of $H_{max}$ for the trivial but physically unrealizable case of $t_d = -t_L$ is infinity; $H_{max}$ then decreases steadily for positively increasing integral values of $t_d/t_L$.

In oscillator configurations I and II above, $t_L = (2t_2 + 2t_3)$ and $t_d = (t_3 + t_4)$. The analysis has shown that the optimal realizable arrangement of these delays under the assumed conditions is with $t_4 = (t_3 + 2t_2)$, in which case $t_d = t_L$ and $H_{max} = 1.00$.

Similarly, the control characteristics of oscillator III may be optimized practically by setting $t_4 = (t_2 + t_3)$, since $t_L = (t_2 + t_3)$ and $t_d = t_4$. Again, $H_{max} = 1.00$.
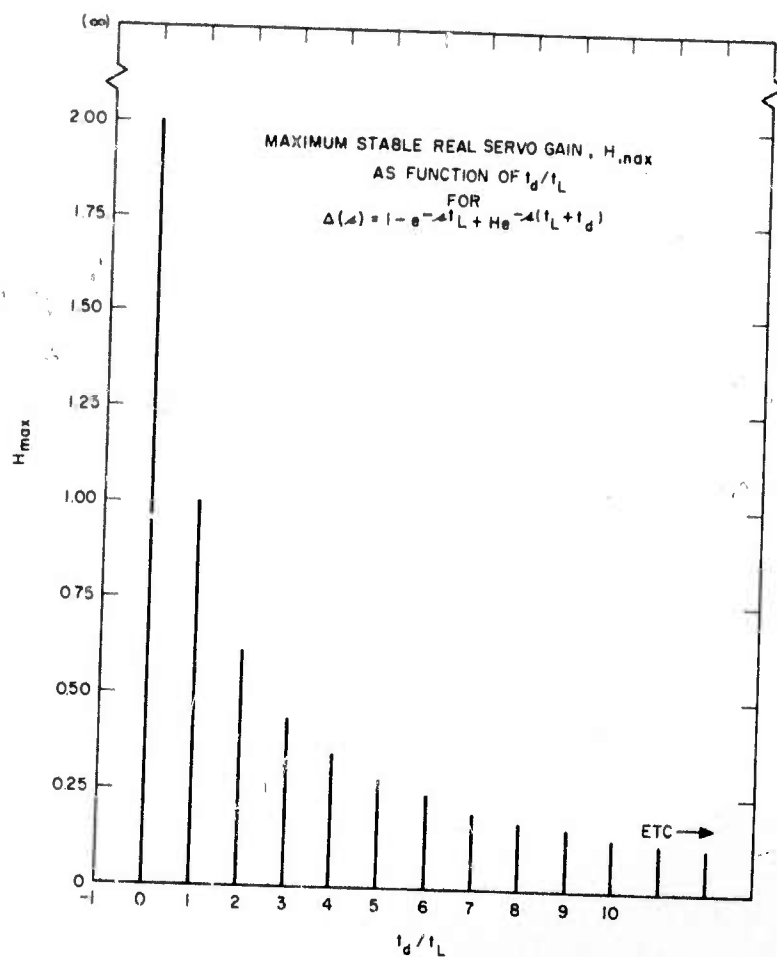
Figure 14. Maximum stable real servo gain, $H_{max}$, as a function of $t_d/t_L$ for $\Delta(\measuredangle) = 1 - e^{-\measuredangle t_L} + He^{-\measuredangle(t_L+t_d)}$.

In oscillators IV and V, $t_L = (t_2 + t_3)$ while $t_d = (t_4 - t_2)$. The possibility of a realizable negative value of $t_d$ is thus apparent. In oscillator IV, one could not achieve $t_2 \geq t_4$ and thus obtain $t_d \leq 0$ without some sort of delay or folding of the main beam between detector beam-splitter and Kerr cell. Without such techniques, the best that can be done (since $t_4 > t_2$) is to set $t_4 = (2t_2 + t_3)$ whereupon $H_{max} = 1.00$ and the control performance should be similar to that of systems I and II as optimized above. If the output beam can be so folded, then setting $t_2 = t_4$ will achieve $t_d = 0$ and $H_{max} = 2.00$, a considerable improvement in performance. The ratio $t_d/t_L$ may be made somewhat negative by

29

making $t_2$ greater than $t_4$; however, according to this analysis the performance would be degraded since the next stable "step", $t_d/t_L = -1$, cannot be attained since mathematically it requires $t_4 = -t_3$.

The configuration of oscillator V facilitates optimal adjustment of the delay $t_2$ so that $t_2 = t_4$. Mathematically, the control performance of this device is identical to that of system IV

From the foregoing discussion it may be concluded that from a control standpoint oscillator V is inherently the most satisfactory of the five devices illustrated. Oscillator IV may be modified to achieve control performance identical to that of V. The first three oscillators may be operated in a stable mode, but their servo gain must be limited to less than unity.

## B. CONTROL CIRCUITRY

The circuit shown in Figure 15 has been constructed in compact form for utilization with the oscillator-amplifier device described in the Optical Design section of this report. This circuit is designed to implement the functions of high-speed servo, integrating servo, and programmed feedback transmission at a single Kerr cell. Use of separate Kerr cells for the program and servo functions would permit a time invariant servo gain and increased electrical efficiency at a price of reduced optical efficiency.

The laser oscillator involved contains a quarter-wave plate and is similar to system I described above. The wollaston prism is oriented such that application of quarter-wave voltage to the kerr cell will result in 100 percent feedback transmission.

Operation of the control circuit is as follows: During the pump period, the tetrodes are biased off at their grids and the net voltage across the Kerr cell is zero. A practical standoff feedback transmission of very nearly zero is thus obtained. Resistors $R_4$ and $R_5$ form a high impedance voltage divider on $V_1$ which insures that tetrode $T_1$ and photodiode D will be initially biased at approximately 5 kv for $V_1 = 10$ kv.

The servo and program drive circuits are triggered at the desired instant of operation. Each of these circuits consists of an 8233 preamp

30

NOMINAL VALUES:

| | | | | |
|---|---|---|---|---|
| $R_1$ = 50 OHMS | $R_6$ = 1 MEG OHM | $C_2$ = 0.001 $\mu f$ | $T_1, T_2$ = TETRODE, 4PR 60B | $V_1$ = 10 kv |
| $R_2$ = 1000 OHMS | $R_{k1}$ = 75 OHMS | $C_3$ = 0.1 $\mu f$ | D = PHOTODIODE (s), FW-114A | $V_2$ = 19 kv. |
| $R_3$ = 2 MEG OHMS | $R_{k2}$ = 75 OHMS | $C_4$ = 0.05 $\mu f$ | K = KERR CELL: $\lambda/4$ = 25 kv; | |
| $R_4$, $R_5$ = 50 MEG OHMS | $C_1$ = 0.001 $\mu f$ | $C_5$ = 0.5 $\mu f$ | CAPACITANCE = 50 pf. | |

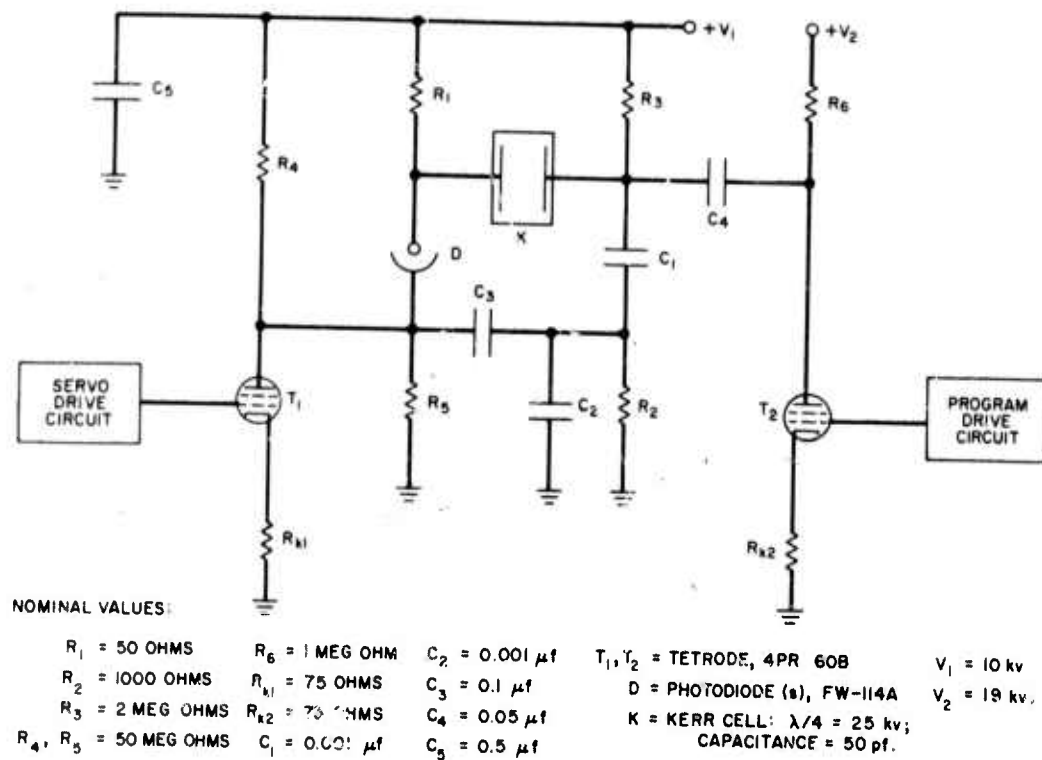Figure 15. Pulse control circuit.

31

tube and an air-cooled 4CX350A power tetrode; typical schematics for these drivers were presented in HAC Report No. P64-24, April 1964. The positive-going waveforms at the grids of tetrodes $T_1$ and $T_2$ bring these tubes out of cutoff and provide drive for the servo reference and program transmission functions respectively. Tetrode $T_1$ is driven at a nominal 5-amp level throughout the controlled pulse; tetrode $T_2$ is driven so as to provide the computed program voltage waveform at the right hand plate of the Kerr cell K. Cathode resistors $R_{k1}$ and $R_{k2}$ are chosen to be as large as possible in order to enhance the constant-current plate characteristics of the tetrodes.

The right hand plate of the Kerr cell will initially swing downward in voltage by an amount equal to the initial program voltage step plus a component resulting from initiation of the servo reference current. Since $C_3 \gg C_2$, the tetrode tends to charge $C_2$ negatively and hence a negative-going voltage is coupled to the Kerr cell through $C_1$.

This strong shutter opening results in immediate commencement of laser oscillation. The monitor photodiode D thus begins to conduct, diverting the tetrode reference current from $C_2$. Since the initial program voltage step alone was presumably sufficient to provide a regenerative loop gain of unity, the negative charge existing on $C_2$ should be removed by an initial overshoot in the output laser power which will cause a current of more than 5 amps to flow through the diode D.

The network D - $T_1$ - $C_3$ - $R_2$ - $C_2$ - $C_1$ provides a slow or "integrating" servo with time constant $R_2 C_2$ when D, $T_1$, and $T_2$ are assumed to be operating as ideal current sources. The finite output impedance of $T_1$ and D appears in parallel with $R_2$ in determining the actual integrator time constant.

With a time constant of 1 $\mu$sec, $R_2$ = 1000 ohms, reference current $I_o$ = 5 amps, regenerative loop transit delay $t_L$ = 10 nanoseconds, $T_o$ = 0.01 percent, and the Kerr cell quarter-wave voltage of 25 kv, an initial effective integrating gain for this servo is achieved of:

$$G_{eff} = G_i \cdot (t_L/\tau) = I_o R_2 \beta \cdot (t_L/\tau) = (5)(10^3)(2.0 \times 10^{-3})(10^{-8})/(10^{-6})$$

$$= 0.10$$

32

This is the fractional amount of correction which has been applied after an "integrating" period of one loop transit time $t_L$. Here $\beta$ is the sensitivity of the Kerr cell involved at $T_o = 0.01$ percent; $\beta = (1/T)(dT/dV)$. During previous analog simulation of the problem an integrator gain of this order of magnitude was shown to be appropriate.

A primary difference in performance between an ideal integrator and this practical RC circuit, neglecting coupling problems at the Kerr cell, is that a residual error in output power will remain after an applied step transmission disturbance of magnitude $\alpha$. The magnitude of the residual error will be approximately

$$\Delta P_r = [1/(G_i + H)] (P_o/T_o)\alpha$$

Here H is the gain of the high-speed servo, $P_o$ is the reference power level, and $T_o$ is the equilibrium Kerr cell feedback transmission. Since $G_i = I_o R_2 \beta = 10.0$ for our system at $T_o = 0.01$ percent, the equilibrium residual error in the output power level should reflect the percent error in program voltage reduced by more than an order of magnitude. With this system, of course, $G_i$ as well as H will decrease during the course of the pulse by a factor of about 4 if the oscillator ruby gain varies from 100 (20 db) to 5 (7 db); or by a factor of about 8 if the terminal point is a ruby gain of 3 db. Hence control during the pulse will be severely degraded without some form of automatic high-speed servo gain variation. Alternatively, a separate Kerr cell could be used for the programmed transmission.

Returning to the circuit diagram, $R_1$ constitutes the load resistor for the fast servo. The value of 50 ohms for $R_1$ will give an initial fast servo gain of H = 0.5 for the operating conditions outlined above. It should be recalled from the analysis that the maximum possible stable fast servo gain for this configuration is H = 1.00; inclusion of the fast time constant (50 ohms x 50 pf = 2.5 nanoseconds = 0.25 $t_L$) as well as the integrator will lower this value considerably.

Capacitors $C_1$ and $C_2$ must shunt the fast servo signal which otherwise would couple to the program side of the Kerr cell through the Kerr cell capacitance. $R_1$ is small enough to perform a similar

function for the program and integrator waveforms on the other side of the Kerr cell.

The coupling network attached to the program or right hand side of the Kerr cell will of necessity reduce the efficiency of the program and integrator servo. Capacitors $C_1$ and $C_2$ will load the program discharge tetrode $T_2$ quite severely for the shorter pulse lengths; yet $C_1$ must be large enough to adequately couple the integrating servo into the Kerr cell despite the loading effect of the tetrode $T_2$. The procedure is to choose $C_1$ to be as large a capacitance as the tetrode can discharge while maintaining a reasonable program waveform. $V_2$ may be set at 19 kv to give a maximum possible program voltage waveform of nearly 18 kv. $C_4$ serves to couple this waveform into the Kerr cell.

$C_5$ is a low-inductance energy-storage capacitor for the servo supply. The network $C_5 - R_1 - K - D - C_1 - C_2 - C_3$ is designed to be as compact as possible to reduce transport delays and series inductance.

The effectiveness of the integrating servo has yet to be experimentally evaluated. The circuit constructed has been operated in the program and fast servo modes by shorting $R_2$ and disconnecting $C_3$.

## IV. HIGH ENERGY CONTROLLED PULSE LASER

### A. GENERAL SYSTEM DESCRIPTION

The basic design of the controlled pulse laser oscillator-amplifier design discussed in the previous section can be scaled up by adding laser elements in parallel to achieve higher energy output. This section will be concerned with a design for a scaled up device which should be capable of delivering from 600 joules to 700 joules output with appropriate control of the pulse length.

Basically the optical design is similar to that used for lower energy and discussed in the previous section. The optical layout is shown in Figure 16. As before the oscillator consist of two high reflectivity (nominally 100 percent) multilayer dielectric reflectors to form the resonant cavity. The active medium of the oscillator are two ruby crystals 5/8 inch in diameter by eight inches long. The optical feedback/output control element as discussed previously is a Kerr cell-Fresnel rhomb - Wollaston prism combination. Decoupling the oscillator and amplifier is accomplished by use of a Faraday rotation isolator and a Kerr cell switch. The beams (one from each oscillator rod) are recollimated to a smaller size before going through the Faraday rotator so that the already developed isolator can be used. The beams are then separated and each expanded in size to fill the aperture of the amplifiers. The amplifier section consists of two bundles each consisting of seven ruby crystals 5/8 inches in diameter by eight inches long. A small portion of the amplifier output energy is split off, expanded, and fed into a high current photodiode to provide the necessary power stabilization signal.

A satisfactory method of physically mounting the optical components of the high energy controlled pulse oscillator-amplifier is shown in Figure 17.

Some of the expected performance characteristics of the controlled pulse oscillator amplifier device are given in Table 1. For a discussion of how these characteristics are obtained, see Appendix B.
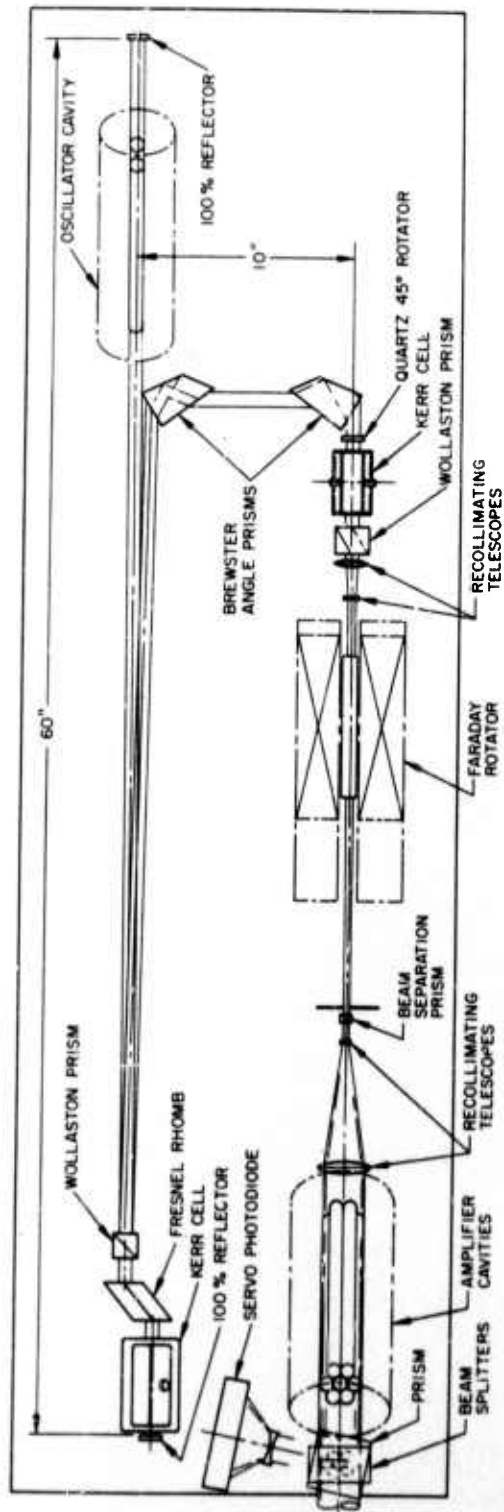
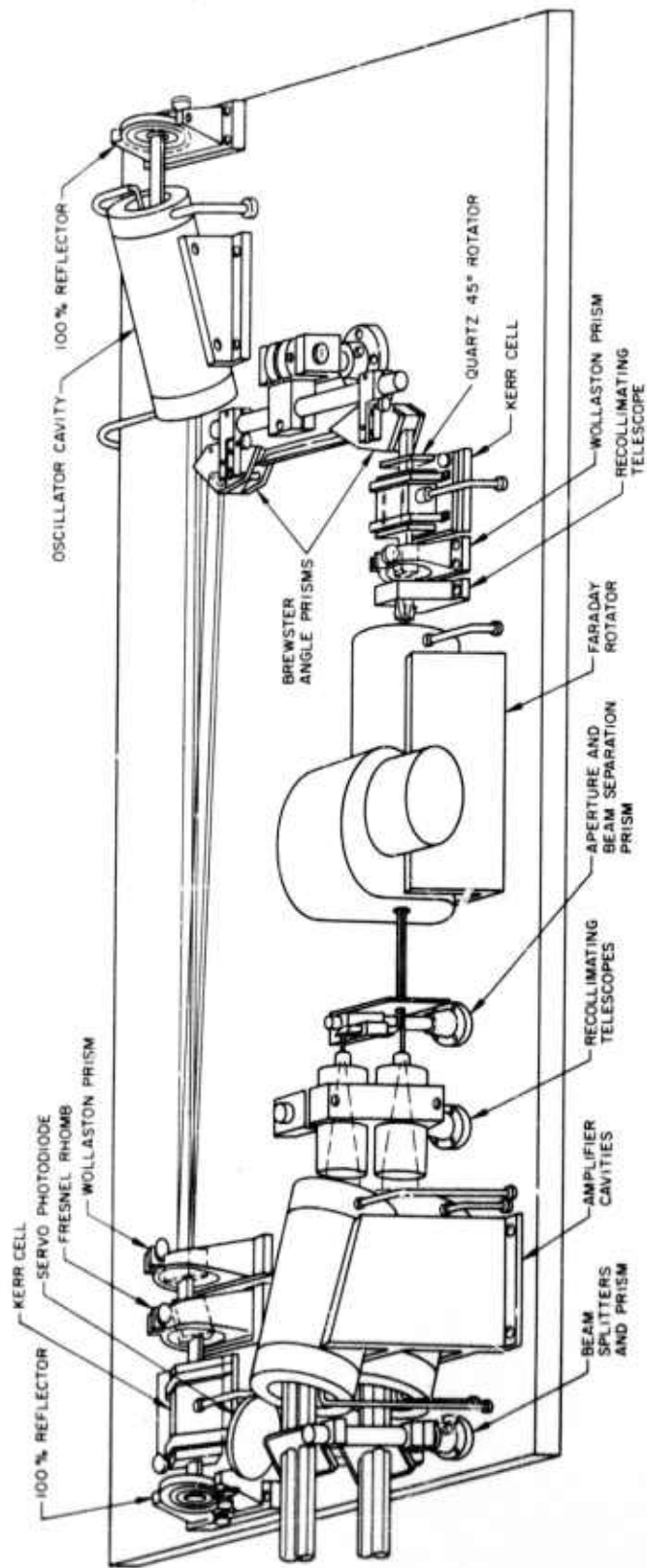Figure 16. High energy controlled pulse oscillator-amplifier optical layout.

36

Figure 17. High energy controlled pulse oscillator-amplifier device.

37

| Osc. Gain | $G_o$ | 20 db | 20 db | 20 db | 20 db | 20 db |
|---|---|---|---|---|---|---|
| Osc. Output Area | $A_o$ | 3.6 cm² (2-5/8" Dia. Rods, 0.9 Effective) | 3.6 cm² (0.9 Effective) | 3.6 cm² (0.9 Effective) | 3.2 cm² (0.8 Effective) | 3.2 cm² (0.8 Effective) |
| Osc. Reflectivity (Effective) | $R$ | 0.8 | 0.8 | 0.8 | 0.9 | 0.9 |
| Coupling Loss | $L$ | 3 db (2) | 1.75 db (1.5) | 3 db (2.0) | 1.75 db (1.5) | 1.75 db (1.5) |
| Amp. Input Area | $A_a$ | 44 cm² | 44 cm² | 44 cm² | 44 cm² | 44 cm² |
| Amp. Effective Area | $A'_a$ | 22.4 cm² 80% of Rod Area | 22.4 cm² 80% of Rod Area | 22.4 cm² 80% of Rod Area | 22.4 cm² 80% of Rod Area | 22.4 cm² 80% of Rod Area |
| Amp. Gain | $G_a$ | 26 db 925 j | 26 db 925 j | 30 db 1070 j | 28 db 1000 j | 28 db 1000 j |
| Initial Regen. | $r(o)$ | $1.25 \times 10^{-4}$ | $1.25 \times 10^{-4}$ | $1.25 \times 10^{-4}$ | $1.11 \times 10^{-4}$ | $1.11 \times 10^{-4}$ |
| Initial K.C. Voltage | $V(o)$ | 2.22 KV | 2.22 KV | 2.22 KV | 2.16 KV | 2.16 KV |
| Final Regen. | $r(t_p)$ | 0.1175 | 0.0212 | 0.00211 | 0.00307 | 0.1175 |
| Final K.C. Voltage | $V(t_p)$ | 12.4 KV | 8.02 KV | 4.5 KV | 4.93 KV | 12.4 KV |
| Output Energy | | 600 j (26.8 j/cm²) | 600 j (26.8 j/cm²) | 600 j (26.8 j/cm²) | 600 j (25.8 j/cm²) | 710 j (32.0 j/cm²) |
| Final Osc. Gain | $Go_f$ | 5.1 db | 8.85 db | 13.86 db | 12.8 db | 5.1 db |
| Peak Power From Osc. | $\frac{Posc}{(t_p)}$ | $\frac{71}{t_p} \frac{Watts}{cm^2}$ | $\frac{53}{t_p} \frac{Watts}{cm^2}$ | $\frac{30.2}{t_p} \frac{Watts}{cm^2}$ | $\frac{39.5}{t_p} \frac{Watts}{cm^2}$ | $\frac{94}{t_p} \frac{Watts}{cm^2}$ |

Table 1. Typical performance characteristics of controlled pulse oscillator — amplifier device.

Superfluorescence in this system is reduced by use of the optical shutter and optical isolator to a negligible level as shown in Appendix D.

## B. OSCILLATOR MULTILAYER DIELECTRIC REFLECTORS

Multilayer dielectric reflectors are suitable for use in the oscillator portion of the device because of the relatively low power levels which are present in the oscillator. As shown in Table 1, depending upon the exact parameters chosen for the system, the peak power of the oscillator varies from $30.2/t_p$ watts/cm$^2$ to $94/t_p$ watts/cm$^2$. For the extreme case of a one-microsecond output pulse, the power level varies from approximately 30 megawatts per square centimeter to 94 megawatts per square centimeter. This is well below the observed damage levels for such dielectric reflectors.

## C. OSCILLATOR PUMPING CAVITY

The oscillator pumping cavity (see Figure 18) is very similar to that used in the low energy controlled pulse laser with the exception that two ruby crystals are utilized instead of a single crystal. In order to pump these two crystals, eight flashtubes are utilized. These flashtubes are similar to the EG&G FX-47 type or the PEK XE-17 series with an eight-inch arc length and one electrode inserted at right angles to the axis of the flashtube.

Fresnel reflection from the ends of the laser crystals are eliminated by use of Brewster angles. Depumping due to the reflections from the periphery of the laser crystals is minimized by immersing the crystals in a glycerol-copper sulphate-water solution. In six-inch long rods of similar cross-sections, gains as high as 22 db have been obtained as shown in Figure 19. Therefore it should be practical to achieve the necessary gain in these rods. In addition, when the rod is immersed, the gain profile across the rod is fairly uniform as demonstrated in Figure 20. This indicates that most of the rod will be effective in emitting energy. In the various cases taken in Figure 18, it was reasonably assumed that either 0.8 or 0.9 of the rod area was effective.
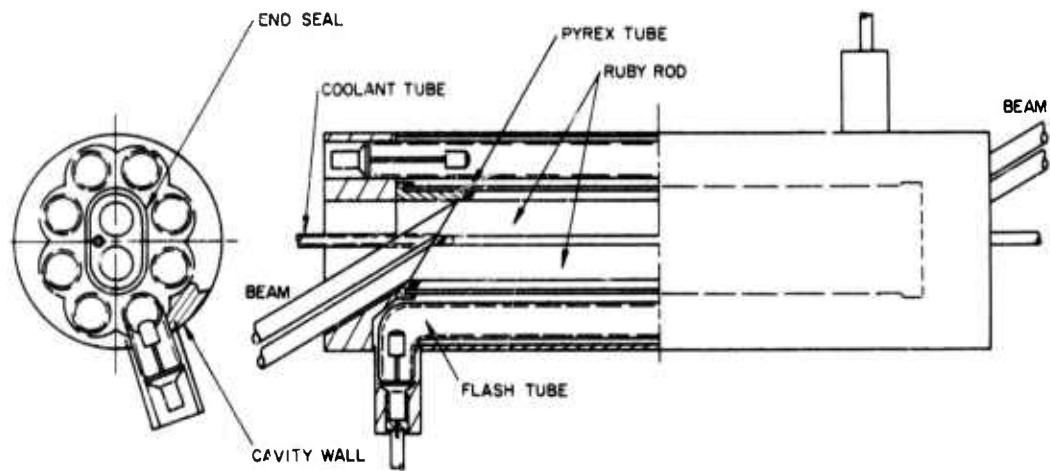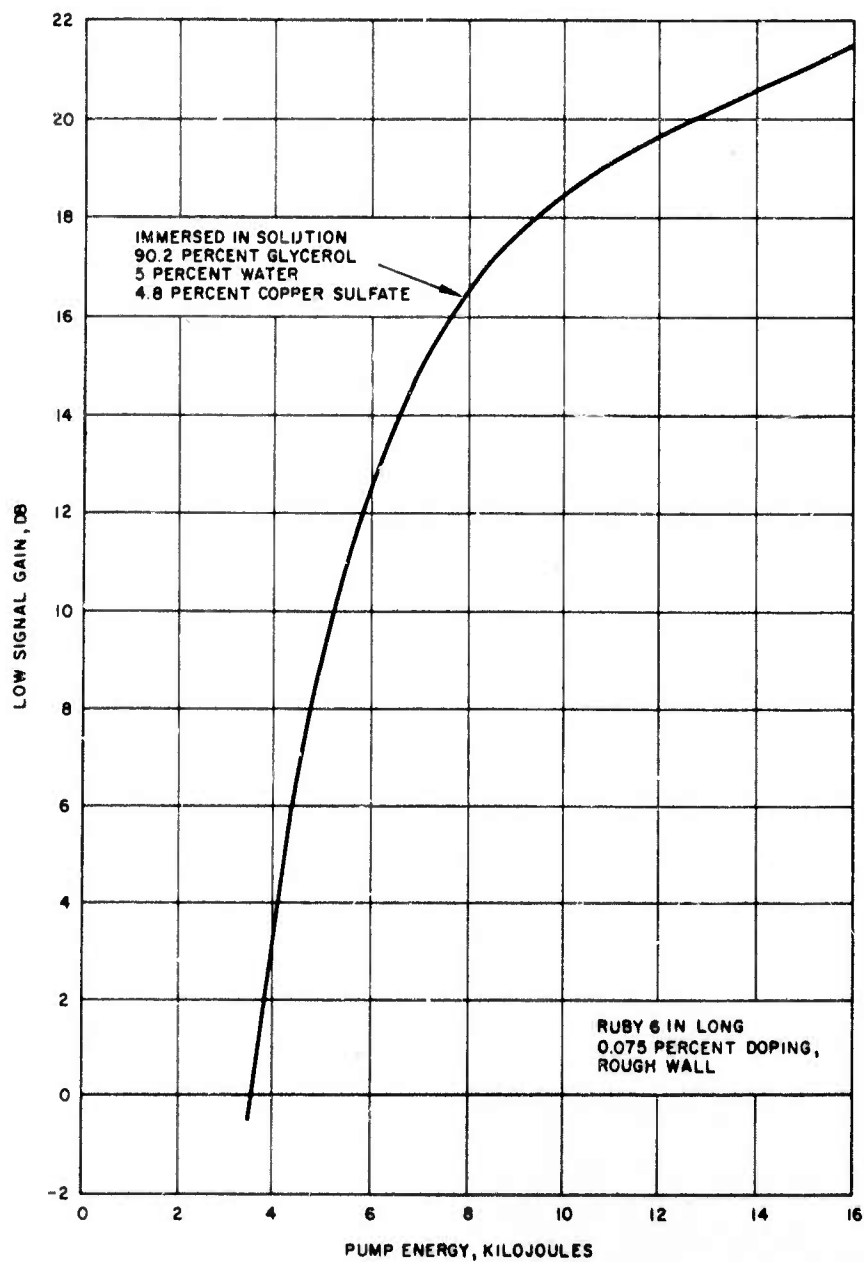
Figure 18. Oscillator pumping cavity.

Figure 19. Amplifier gain versus input energy.

41
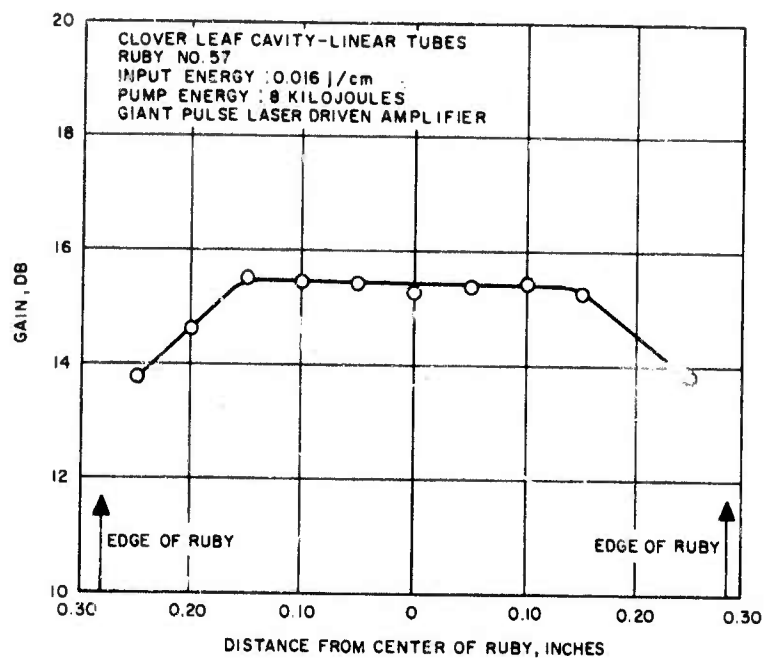
Figure 20. Gain versus probe position.

42

## D. OPTICAL FEEDBACK-OUTPUT SWITCH

The Kerr cell - Fresnel rhomb - Wollaston prism optical feedback output switch is identical to that used in the lower energy device. As mentioned in a previous section, the "off" transmission of this switch is less than $10^{-4}$, which is adequate for operation of the oscillator crystals at 20 db single pass gain.

## E. OPTICAL ISOLATOR

The characteristics of the optical isolator have been reported previously (see HAC TP-64-24). In summary an isolation of approximately 30 db has been achieved with an insertion loss of approximately ..5 db.

## F. KERR CELL SWITCH

The Kerr cell optical switch is used to isolate the oscillator and amplifier during the pump phase. With voltage off, the condition during the pump phase, the switch provides better than 40 db isolation in both directions. Half wave voltage is applied to the Kerr cell at the initiation of the controlled pulse laser sequence to couple the oscillator and amplifier. The losses in the switch with half-wave voltage on appears to be negligible.

## G. AMPLIFIER PUMPING CAVITY

The amplifier pumping cavity design is shown in Figure 21. Two amplifier sections are used in parallel, each consisting of seven ruby crystals pumped by twelve flashtubes. The ruby crystals and flashtubes are identical to those used in the oscillator. Similarly, the ends of the ruby are cut at Brewster angle; the periphery of the crystal roughened, and the crystal immersed in the glycerol-copper sulphate-water solution.

## H. SERVO PHOTODIODE

In order to obtain a larger current to perform the control function, a five-inch diameter S-20 biplanar photodiode is used instead of

43

two-inch diameter tube used in the lower energy device. This tube is
capable of delivering up to 30 amperes at the voltage necessary to per-
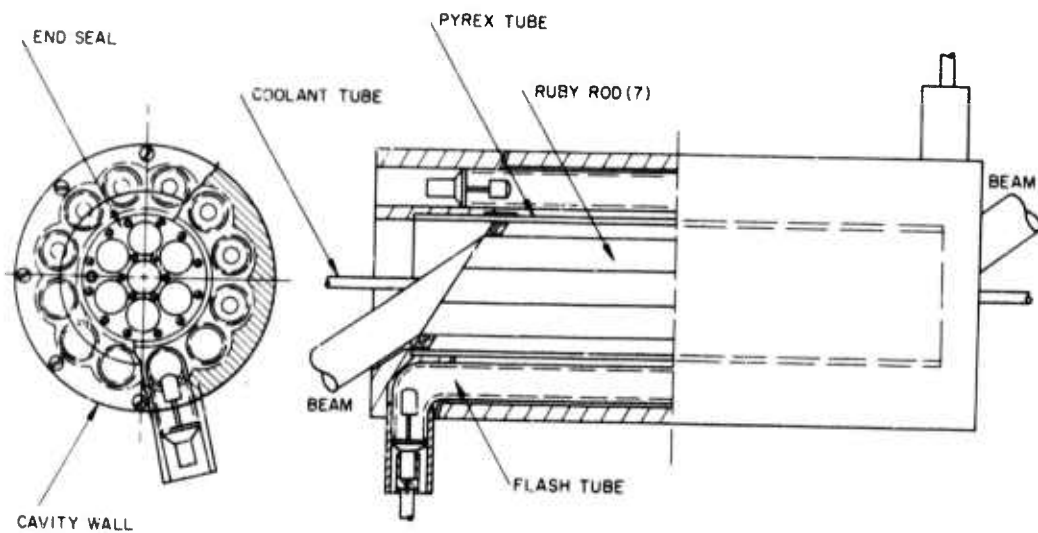form the control function.



Figure 21. Amplifier pumping cavity.

# APPENDIX A

## FRESNEL RHOMB

Light incident upon the dielectric rhomboid, as shown in Figure A-1, undergoes two total internal reflections at angles of incidence $\theta$. The phase of the perpendicular and parallel polarization components are shifted by $\delta_\perp$ and $\delta_{||}$ upon reflection. The following equations determine these phase shifts.
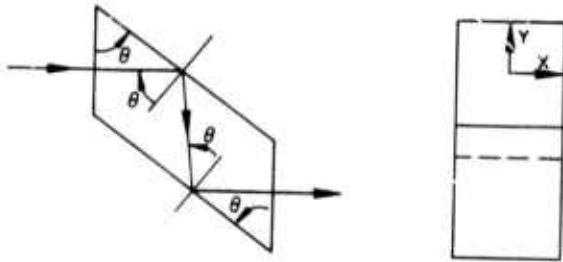


Figure A-1. Fresnel rhomb.

$$\tan\left(\frac{\delta_\perp}{2}\right) = \frac{\sqrt{n^2 \sin^2\theta - 1}}{n \cos\theta} \qquad \text{(phase shift of } E_x\text{)} \qquad (1)$$

$$\tan\left(\frac{\delta_{||}}{2}\right) = \frac{n\sqrt{n^2 \sin^2\theta - 1}}{\cos\theta} \qquad \text{(phase shift of } E_y\text{)} \qquad (2)$$

For a partial wave plate the differential phase shift $\delta_{||} - \delta_\perp$ is the pertinent quantity. This can be expressed via the trigonometric identity:

$$\tan\left(\frac{\delta_{||} - \delta_\perp}{2}\right) = \tan\left(\frac{\Delta}{2}\right) = \frac{\tan\left(\frac{\delta_{||}}{2}\right) - \tan\left(\frac{\delta_\perp}{2}\right)}{1 + \tan\left(\frac{\delta_{||}}{2}\right)\tan\left(\frac{\delta_\perp}{2}\right)} \qquad (3)$$

or:

$$\tan\left(\frac{\Delta}{2}\right) = \left(\frac{n^2 - 1}{n}\right)\frac{f}{1 + f^2} \qquad ; \qquad f = \frac{\sqrt{n^2 \sin^2\theta - 1}}{\cos\theta} \qquad (4)$$

The rate of change of the relative phase shift, $\Delta$, with angle of incidence, $\theta$, is given by:

$$\frac{d\Delta}{d\theta} = \frac{2\left(\frac{n^2 - 1}{n}\right)}{1 + \left[\left(\frac{n^2 - 1}{n}\right)\frac{f}{1 + f^2}\right]^2}\left[\frac{1}{1 + f^2} - 2\left(\frac{f}{1 + f^2}\right)^2\right]\left(f + \frac{n^2}{f}\right)\tan\theta \tag{5}$$

As an example, for $\Delta = \pi/4$ (total relative phase shift through the rhomb $= \pi/2$, thus a quarter wave plate) and $n = 1.5$ the requisite value of $\theta$ is 53 degrees. The rate of change of $\Delta$ with orientation is very small in this case -- $d\Delta/d\theta = 0.249$ -- but this is because we are near the peak of the $\Delta$ vs $\theta$ curve. At $f = 1$, $d\Delta/d\theta = 0$. This peak occurs at $\Delta/2 = 22$ degrees 30 minutes for $n \cong 1.497$, which is the minimum index for which this device will work as a quarter wave plate, and the corresponding angle of incidence is $\theta = 51$ degrees 49 minutes.

## Effects of Errors in Alignment

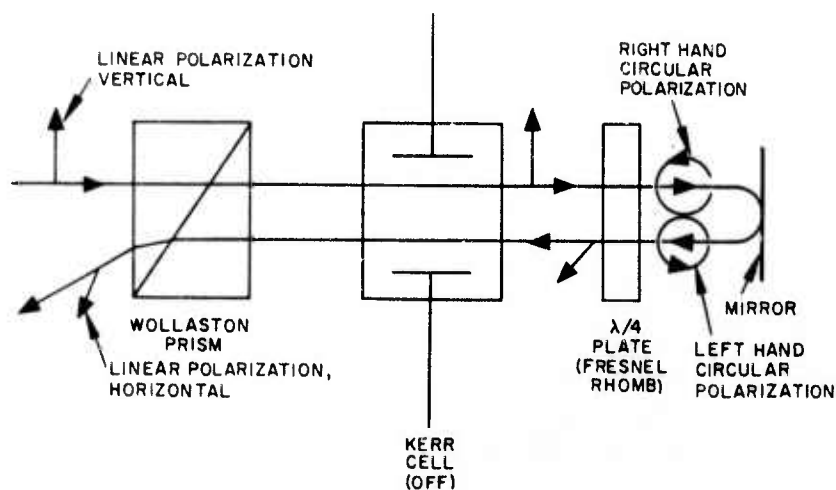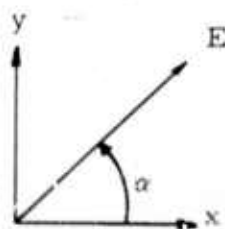We want to use the rhomb in a switch as in Figure A-2.



Figure A-2. Optical switch with quarter-wave plate.

Alignment errors permit some of the signal to return along its incident path. We consider a linear polarized beam incident on a quarter-wave plate.



$$\alpha = \frac{\pi}{4} + \delta$$

46

<u>IN</u> to λ/4 plate
(going to right)

$$E_x = E \cos \alpha$$
$$E_y = E \sin \alpha$$

<u>OUT</u> of λ/4 plate
(going to right)

$$E_x = E \cos \alpha$$
$$E_y = E \sin \alpha \, e^{i2\Delta} \; : \; \Delta = \pi/4 + \epsilon$$

<u>IN</u> to λ/4 plate
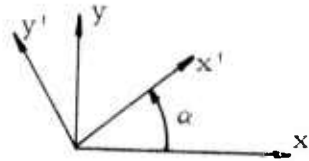(going to left)

$$E_x = E \cos \alpha$$
$$E_y = E \sin \alpha \, e^{i2\Delta}$$

<u>OUT</u> of λ/4 plate

$$E_x = E \cos \alpha$$
$$E_y = E \sin \alpha \, e^{i4\Delta}$$

Thus, after this double pass the field along the original direction is given by:



$$E_x' = E_x \cos \alpha + E_y \sin \alpha$$
$$E_y' = -E_x \sin \alpha + E_y \cos \alpha$$

So:

$$E_x' = E(\cos^2 \alpha + \sin^2 \alpha \, e^{i4\Delta})$$

Then:

$$P' = P(\cos^4 \alpha + \sin^4 \alpha + 2 \sin^2 \alpha \cos^2 \alpha \cos 4\Delta)$$

or, the transmission coefficient can be written

$$T = \cos^4 \alpha + \sin^4 \alpha + 2 \cos^2 \alpha \sin^2 \alpha + 2 \quad s^2 \alpha \sin^2 \alpha (\cos 4\Delta - 1)$$

Thus:

$$T = 1 + \frac{1}{2}(\sin^2 2\alpha)(\cos 4\Delta - 1)$$

Inserting

$$\alpha = \frac{\pi}{4} + \epsilon \text{ and } \Delta = \frac{\pi}{4} + \delta \qquad ; \qquad \epsilon, \, \delta \ll 1$$

47

we get:

$$T \cong (2\delta)^2 + (2\epsilon)^2$$

From this we see that for 40 db isolation ($T = 10^{-4}$) we need the quarter wave plate axes properly aligned to within $\epsilon = 1/2 \times 10^{-2}$ rad. The single transit relative phase shift error ($2\delta$) must be less than $10^{-2}$ rad. Neither of these requirements are severe. For the case $n = 1.5$, $0 = 53$ degrees the required accuracy in $0$ is $2 \times 10^{-2}$ rad, or about 1 degree.

Conclusion: By using an index of refraction only slightly higher than the cut-off value, $n = 1.497$, the $\theta$-alignment accuracy is non-critical. The x-y alignment is always non-critical.

### Switch Operation

We take the switch to be composed of a polarizer followed by a Kerr cell canted at 45 degrees to the polarizer, a quarter wave plate aligned with the Kerr cell and a plane mirror.
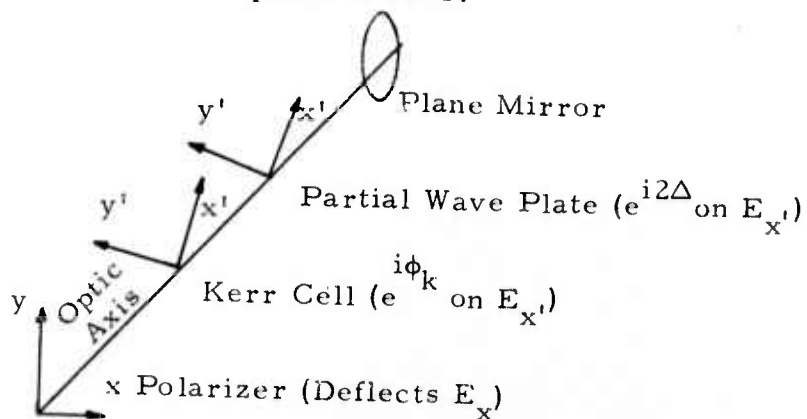


Since the polarizer possesses only the y-component the input to the Kerr cell is

$$E_x' = E_y/\sqrt{2} \qquad ; \qquad E_y' = E_y/\sqrt{2} \ .$$

After passing through the elements the output from the Kerr cell is

$$E_x' = \frac{E_y}{\sqrt{2}} e^{i(2\phi_k + 4\Delta)}$$

$$E_y' = \frac{E_y}{\sqrt{2}}$$

Through the polarizer we have

$$E_y^O = \frac{E_x' + E_y'}{\sqrt{2}} \qquad ; \qquad E_x^O = \frac{E_x' - E_y'}{\sqrt{2}}$$

So:

$$E_y^O = \frac{E_y}{2}\left[1 + e^{i(2\phi_k + 4\Delta)}\right]$$

$$E_x^O = \frac{E_y}{2}\left[-1 + e^{i(2\phi_k + 4\Delta)}\right]$$

Then, the transmission factor is:

$$T = \frac{E_y^O E_y^{O*}}{E_y E_y^*} = \frac{1}{2}\left[1 + \cos(2\phi_k + 4\Delta)\right]$$

and the deflection factor is

$$D = 1 - T = \frac{1}{2}\left[1 - \cos(2\phi_k + 4\Delta)\right]$$

For a quarter wave plate, $\Delta = \pi/4$, we get

$$T = \frac{1}{2}\left[1 - \cos 2\phi_k\right]$$

# APPENDIX B

## OPERATION OF CONTROLLED PULSE
## OSCILLATOR-AMPLIFIER

The optical circuit under consideration is schematically shown in Figure B-1.
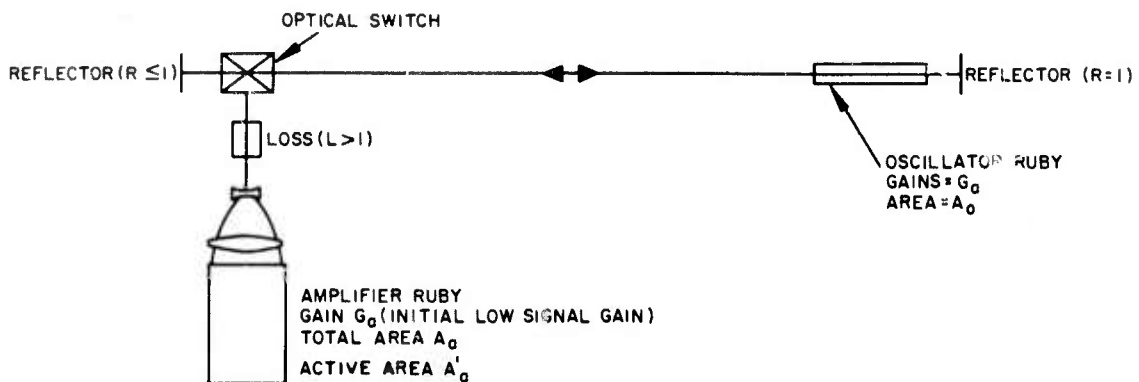


Figure B-1. Optical schematic.

The optical switch deflects a fraction $(1 - r(t))$ of the oscillator circulating power into the output channel, the amplifier arm. The rest of the oscillator beam $(r(t))$ is fed back. The loss term is inserted to accommodate optical inefficiencies which will be present to some extent in the coupler and lenses.

The amplifier is considered to be non-regenerative (say by the use of Brewsters' angle faces), so the integrated output energy $W_o (j/cm^2)$ can be related to the input energy $W_i (j/cm^2)$ by the following equation:

$$\frac{e^{W_i/\Omega} - 1}{e^{W_o/\Omega} - 1} = \frac{1}{G_a} \qquad ; \qquad \Omega = 6.9 \, j/cm^2 \quad \text{for room temperature ruby}$$

(1)

or

$$\frac{W_i(t)}{\Omega} = \ln \frac{e^{W_o/} - 1}{G_a} + 1$$

(2)

Since the desired output power is constant, we can take

$$W_o = P_o t \quad ; \quad P_o \text{ in watts/cm}^2 \tag{2a}$$

Then differentiating Equation (2) with respect to time, we get the requisite input power:

$$\frac{P_i(t)}{\Omega} = \frac{P_o}{\Omega} \left[ \frac{\exp(P_o t/\Omega)}{\exp(P_o t/\Omega) - 1 + G_a} \right] \quad ; \quad P_i(t) \text{ in watts/cm}^2 \tag{3}$$

This, then, must be supplied by the oscillator. Because of the loss and the recollimation, the oscillator output flux (watts/cm$^2$) must be

$$\frac{P_{osc}(t)}{\Omega} = \frac{P_i(t)}{\Omega} \left( \frac{A_a}{A_o} L \right) \tag{4}$$

Thus:

$$\frac{P_{osc}(t)}{\Omega} = \left( \frac{A_a}{A_o} L \right) \frac{P_o}{\Omega} \frac{e^{P_o t/\Omega}}{e^{P_o t/\Omega} - 1 + G_a} \tag{5}$$

Next consider what $r(t)$ must be to yield $P_{osc/\Omega}(t)$. The internal losses in the oscillator are approximately represented by the less than unity value of R, the reflector at the left end. If we assume that some sort of mode selector is located at that end, then the radiation scattered in the rod will be eliminated or lost. The power thus lost, $P_\ell(t)$, can be related to the oscillator output through:

$$P_\ell(t) = P_{osc}(t) \left[ \frac{1 - R}{(1 - r(t))R} \right] \tag{6}$$

However, since $r(t) \ll 1$ for most cases of interest, we can say that

$$P_\ell(t) + P_{osc}(t) \cong \frac{P_{osc}(t)}{R} \tag{7}$$

52

This is the total power drain from the oscillator. Thus the energy extracted from the oscillator ruby is

$$\frac{W_{ext}}{\Omega} = \int_0^t \frac{P_{osc}(t)}{R\Omega} \, dt$$

Now the requisite value of r(t), for a slowly changing pulse is given approximately by:

$$r(t) = \frac{1}{RG^2(t)} \tag{8}$$

where the instantaneous rod gain is related to the initial gain by:

$$G(t) \cong G_o \exp(-W_{ext}/\Omega) \tag{9}$$

$$= G_o \exp\left[-\int_0^t \frac{P_{osc}(t)}{R\Omega} \, dt\right] \tag{10}$$

Then:

$$r(t) \cong \frac{1}{RG_o^2} \exp\left[2\int_0^t \frac{P_{osc}(t)}{R} \, dt\right] \tag{11}$$

The justification for Equation (8) is given in Appendix C. After inserting Equation (5) for $P_{osc}(t)$, and performing the integration, this yields:

$$R(t) \cong \frac{1}{RG_o^2} \exp\left\{\left(\frac{2A_a L}{RA_o}\right)\ln\left[\frac{e^{P_o t/\Omega} - 1 + G_a}{G_a}\right]\right\} \tag{12}$$

(which relates to voltage through $r(t) = \sin^2(kv^2(t))$ ($k = 22.7 \times 10^{-10}$ typically)).

In Figure B-2 a plot of $r(t)$ versus the parameter $P_o t/\Omega$ for $\sqrt{RG_o} = 100$, $G_a = 400$, $A_a/A_o = 9.1$ and several different values of $L/R$ ($= 2, 4, 8$) are shown. It is indicated at the bottom of this curve what this means in terms of total output energies for two different values of effective output area. Figure B-3 translates $r(t)$ to $V(t)$, the voltage on the oscillator Kerr cell.

Equation (12) indicates that following the turn on phase of the operation, $r(t)$ must start out at the value $r(o) = 1/RG_o^2$. The f      value of $r(t)$ depends upon the desired energy extraction. Following this we list some special cases in which $r_{FINAL}$ is shown.
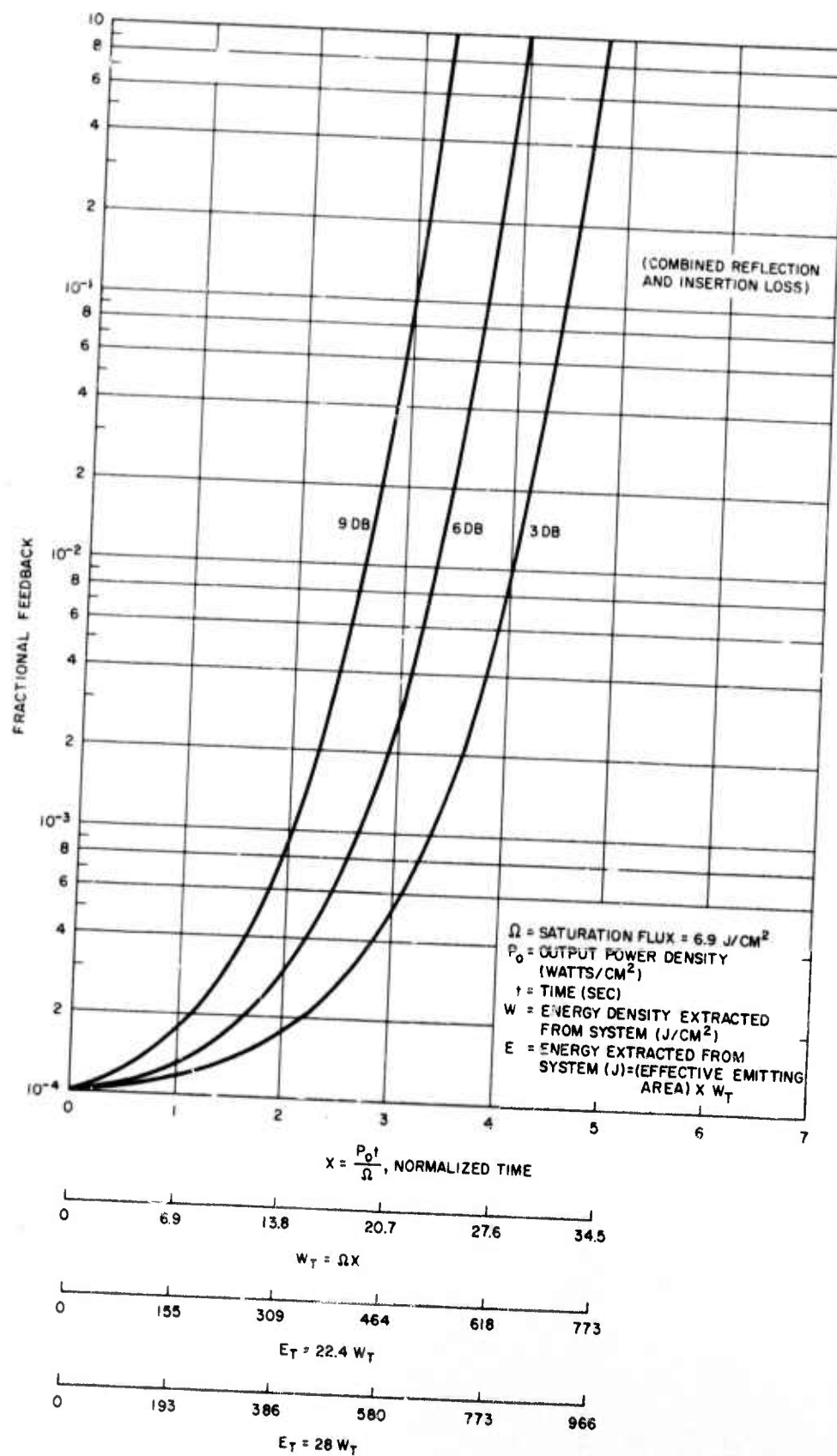
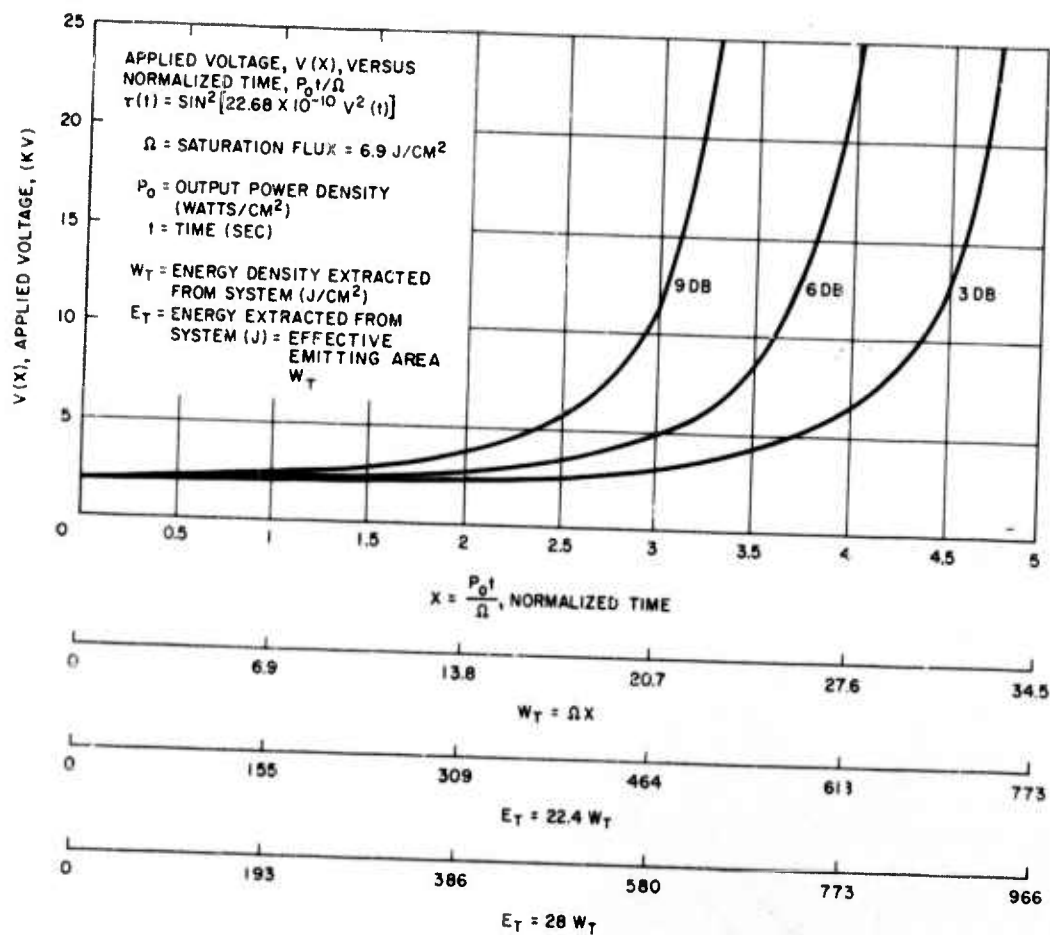Figure B-2. Fractional feedback versus normalized time.

55

Figure B-3. Kerr cell voltage versus normalized time.

The chart contains the following labels and annotations:

- Y-axis: $V(X)$, APPLIED VOTAGE, (KV) — with values 0, 5, 10, 15, 20, 25
- X-axis: $X = \dfrac{P_0 t}{\Omega}$, NORMALIZED TIME — with values 0.5, 1, 1.5, 2, 2.5, 3, 3.5, 4, 4.5, 5

Text box:

APPLIED VOLTAGE, $V(X)$, VERSUS NORMALIZED TIME, $P_0 t/\Omega$

$\tau(t) = \mathrm{SIN}^2 \left[ 22.68 \times 10^{-10} \, V^2(t) \right]$

$\Omega$ = SATURATION FLUX = 6.9 J/CM$^2$

$P_0$ = OUTPUT POWER DENSITY (WATTS/CM$^2$)

$t$ = TIME (SEC)

$W_T$ = ENERGY DENSITY EXTRACTED FROM SYSTEM (J/CM$^2$)

$E_T$ = ENERGY EXTRACTED FROM SYSTEM (J) = EFFECTIVE EMITTING AREA $W_T$

Curve labels: 9 DB, 6 DB, 3 DB

Additional scales:

$W_T = \Omega X$: 0, 6.9, 13.8, 20.7, 27.6, 34.5

$E_T = 22.4 \, W_T$: 0, 155, 309, 464, 613, 773

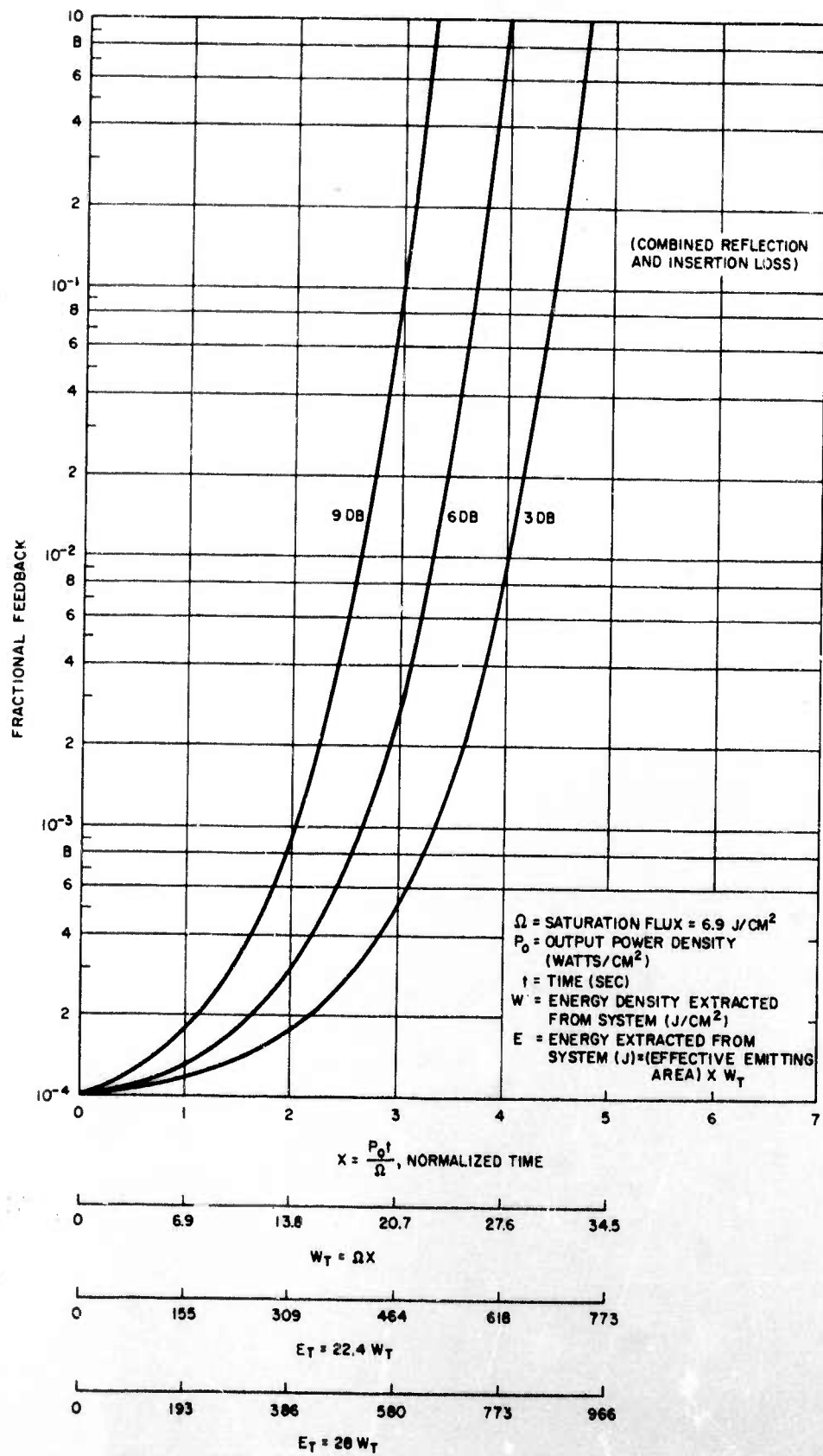$E_T = 28 \, W_T$: 0, 193, 386, 580, 773, 966

Figure B-2. Fractional feedback versus normalized time.

# APPENDIX C

## JUSTIFICATION OF THE EQUATION $r(t) = \dfrac{1}{RG^2(t)}$

Referring back to Equation (8) in Appendix B, we can write a more precise finite difference equation relating $r(t)$ and $G(t)$, as follows:



$$P_{osc}(t) \equiv p(t) \qquad\qquad\qquad G(t)$$

$$p(t + t_L) = p(t)\left(\frac{r(t)}{1 - r(t)}\right) G^2\left(t + \frac{t_L}{2}\right) R(1 - r(t + t_L)) \tag{1}$$

Then:

$$r(t) = \left(\frac{p(t + t_L)}{p(t)}\right)\left(\frac{1 - r(t)}{1 - r(t + t_L)}\right) \frac{1}{RG^2(t)} \left(\frac{G^2(t)}{G^2(t + t_{L/2})}\right) \tag{2}$$

The justification of the title equation of course is that the three terms in brackets are all about unity. This is next shown:

$$p(t + t_L) \cong p(t) + t_L \frac{dp(t)}{dt} \tag{3}$$

$$\frac{p(t + t_L)}{p(t)} = 1 + t_L \frac{1}{p(t)} \frac{dp(t)}{dt} \tag{4}$$

Using:

$$p(t) = \left(\frac{A_a L}{A_o}\right) p_o \frac{e^{p_o t/\Omega}}{e^{p_o t/\Omega} - 1 + G_a} \tag{5}$$

57

We get:

$$\frac{dp(t)}{dt} = \left(\frac{A_a L}{A_o}\right) P_o \frac{P_o}{\Omega} \frac{e^{P_o t/\Omega}}{e^{P_o t/\Omega} - 1 + G_a} \left[1 - \frac{e^{P_o t/\Omega}}{e^{P_o t/\Omega} - 1 + G_a}\right] \quad (6)$$

So:

$$\frac{1}{p(t)} \frac{dp(t)}{dt} = \frac{P_o}{\Omega} \left[\frac{G_a - 1}{e^{P_o t/\Omega} + G_a - 1}\right] \quad (7)$$

The term in brackets is about unity since $G_a \gg e^{P_o t/\Omega}$. Also, the operation of this device is in the range

$$\frac{P_o t_p}{\Omega} \cong 3 \text{ or } 4 \quad (8)$$

and:

$$t_L \frac{1}{p(t)} \frac{dp(t)}{dt} = (3 \text{ or } 4) \times \frac{t_L}{t_p} \quad (9)$$

Since $t_L = 5 \times 10^{-9}$ sec. and $t_p$ is in the range $10^{-6}$ to $10^{-4}$ sec this is indeed a small term.

Next:

$$\frac{1 - r(t)}{1 - r(t + t_L)} = 1 + t_L \left(\frac{\frac{dr}{dt}}{1 - r(t + t_L)}\right) \quad (10)$$

Since $r(t)$ is in almost all circumstances $\ll 1$ the denominator in the brackets can be dropped.

Using:

$$r(t) \cong \frac{1}{RG_o^2} \exp\left\{\left(\frac{2A_a L}{RA_o}\right) \ln\left[\frac{e^{P_o t/\Omega} - 1 + G_a}{G_a}\right]\right\}$$ (11)

$$\frac{dr(t)}{dt} = r(t) \frac{P_o}{\Omega} \left(\frac{2A_a L}{RA_o}\right)\left[\frac{e^{P_o t/\Omega}}{e^{P_o t/\Omega} - 1 + G_a}\right]$$ (12)

$$< \frac{1}{10} \quad \sim 4/t_p \quad \sim 60 \quad \sim \frac{1}{10}$$

So:

$$t_L \frac{dr(t)}{dt} \sim \text{several} \times \frac{t_L}{t_p}$$ (13)

which is, once again, negligible.

Finally, the last term in Equation (2) can be written:

$$\frac{G^2(t)}{G^2\left(t + \frac{t_L}{2}\right)} = \frac{1}{1 + \left(\frac{1}{G(t)} \frac{dG(t)}{dt}\right) t_L}$$ (14)

Using:

$$G(t) = G_o \exp\left\{-\left(\frac{A_a L}{RA_o}\right)\ln\left[\frac{e^{P_o t/\Omega} - 1 + G_a}{G_a}\right]\right\}$$ (15)

We obtain:

$$\frac{d \ln G(t)}{dt} = -\left(\frac{A_a L}{RA_o}\right)\left[\frac{e^{P_o t/\Omega}}{e^{P_o t/\Omega} - 1 + G_a}\right]\frac{P_o}{\Omega}$$ (16)

$$\sim 30 \quad \sim \frac{1}{10} \quad \sim 4/t_p$$

59

Thus:

$$t_L \frac{1}{G(t)} \frac{dG(t)}{dt} \sim (\text{ten or so}) \times \frac{t_L}{t_p} \tag{17}$$

This is slightly larger than the previous term, but still negligible. It is, therefore, correct to say that the transmission function $r(t)$ is given approximately by

$$r(t) \cong \frac{1}{RG^2(t)} \tag{18}$$

# APPENDIX D

## SUPERFLUORESCENCE EFFECTS

The circuit under consideration is the optical equivalent of Figure D-1.
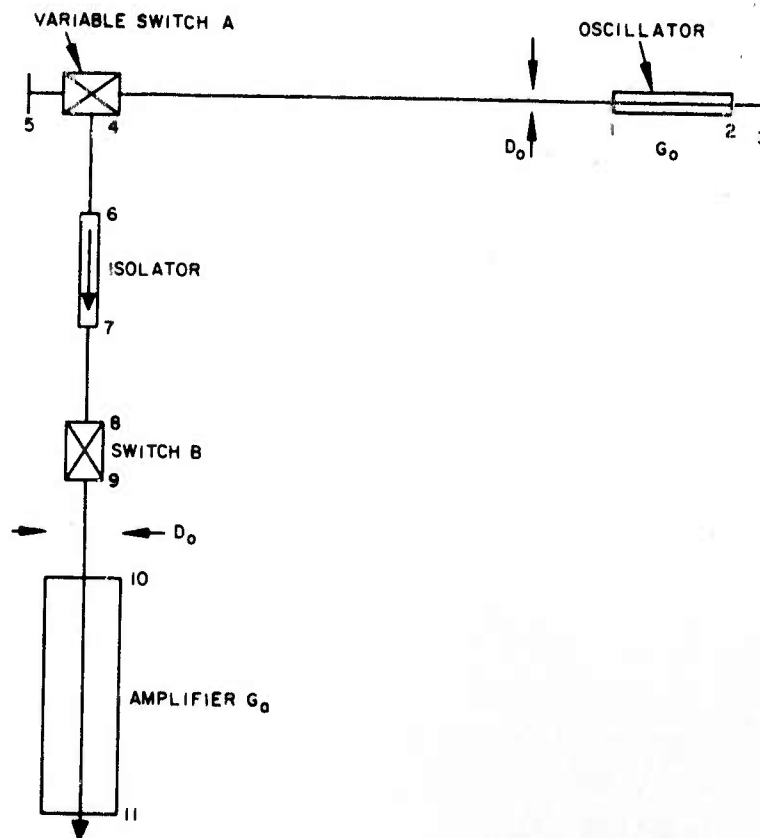


Figure D-1.  Superfluorescence paths.

Hughes is concerned with the superfluorescence problem in two circumstances: (1) during the pump period when both switches A and B are fully off and (2) during the output period when switch B is fully open and switch A is slowly opening. Case (1) is considered first.

(1) The straight superfluorescence path here is $1 \to 2 \to 3 \to 2 \to 1$. There is no reflection at either ruby face (Brewster's angle cut). The fluorescent decay is taken to be isotropic and completely $\sigma$-polarized. Present evidence indicates that this is an adequate approximation. The fluorescence will be further simplified by using a two level model of ruby and neglecting the $R_2$ line.

$$\underline{\hspace{3cm}} \quad N_e$$

$$N_e + N_g = N_o$$

$$\underline{\hspace{3cm}} \quad N_g$$

With the two level model the rate equation for the excited population at a point $X'$ is given by

$$\frac{dN_e}{dt} = -[2N_e - N_o] \int \sigma g(\nu)\mu(\nu) \, d\nu - \frac{N_e}{\tau} + (N_o - N_e)W_{ge} \tag{1}$$

where $W_{ge}$ is the pumping rate $(\sec^{-1})$. To put this in perspective for the contemplated application, the case of 0.075 percent ruby, 6" long with 23 db gain is taken. Thus,

$$N_e = 2.03 \times 10^{19} \text{ ions/cm}^3 = 0.86 \, N_o$$

$$N_o = 2.37 \times 10^{19} \text{ ions/cm}^3 \tag{2}$$

So, roughly:

$$\frac{dN_e}{dt} = -N_e \left[ \frac{1}{\tau} + \underbrace{0.83 \int \sigma g(\nu)\mu(\nu) \, d\nu}_{\equiv I} - 0.17 \, W_{ge} \right] \tag{3}$$

62

Thus, the effect of superfluorescence is to shorten the effective decay time.

To calculate $\mu(\nu)$ the rate of decay from a slab dX thick at the X-plane is looked at first. This is:

$$\frac{dm(\nu)}{dt} = \frac{\pi R^2(x)\,dX}{\tau}\, N_e Ag(\nu)\,d\nu \quad \text{photon/sec in } d\nu \tag{4}$$

where $\pi R^2(X)$ is the cross sectional area of the rod at the X-plane, $\tau$ is the decay time and

$$Ag(\nu) = A \exp\left[-\left(2\sqrt{\ln 2}\right)^2\left(\frac{\nu - \nu_0}{\Delta\nu}\right)^2\right]\; ; \tag{5}$$

(Gaussian line)

$$A = \frac{2}{\Delta\nu}\sqrt{\frac{\ln 2}{\pi}}\; ; \qquad \int_0^\infty Ag(\nu)\,d\nu = 1 \tag{6}$$

$$\Delta\nu = \text{R}_1 \text{ line half width}$$

If the output solid acceptance angle is $\Omega(X)$ at the X-plane then the fraction of photons in Equation (4) which contributes to superfluorescence at the output is

$$\frac{\Omega(X)}{4\pi}$$

Thus the spectral flux at the output face, from dX, is given by

$$d\mu(\nu) = \frac{N_e}{\tau}\,\frac{\Omega(X)}{4\pi}\,\frac{2}{\Delta\nu}\sqrt{\frac{\ln 2}{\pi}}\,g(\nu)\,G(X)\,\frac{\pi R^2(X)}{\pi R^2(L)}\,d\nu\,dX \tag{7}$$

The contribution from the initiating end will be dominant since it experiences the greatest gain, $G(X)$. For this reason:

$$\Omega(X)\frac{\pi R^2(X)}{\pi R^2(L)} = \Omega(0)\frac{\pi R^2(0)}{\pi R^2(L)} \tag{8}$$

63

Integrating over G(X) one gets

$$\mu(\nu) = \frac{N_e}{\sigma \tau} \frac{\Omega(0)}{4\pi} \frac{A(0)}{A(L)} \frac{2}{\Delta \nu} \sqrt{\frac{\ln 2}{\pi}} \frac{G_o(\nu)}{2N_e - N_o} d\nu \tag{9}$$

$$\text{photons/cm}^2 \text{ sec in } d\nu$$

Next, one needs to evaluate

$$I = \int \sigma g(\nu) \mu(\nu) \, d\nu$$

$$= \frac{N_e}{2N_e - N_o} \frac{\Omega(0)}{4\pi} \frac{A(0)}{A(L)} \frac{1}{\tau} \frac{2}{\Delta \nu} \sqrt{\frac{\ln 2}{\pi}} \int g(\nu) \exp\left[\sigma g(\nu)(2N_e - N_o)L\right] d\nu \tag{10}$$

The integral in this expression is very difficult to evaluate. It is approximated by taking

$$\int g(\nu) \exp\left[\sigma g(\nu)(2N_e - N_o)L\right] d\nu = G_o \delta \nu \tag{11}$$

where $\delta \nu$ is the half-width of the saturation narrowed line. For high gain this is given by, approximately

$$\frac{\delta \nu}{\Delta \nu} \cong \frac{1}{\sqrt{\ln G_o}} \tag{12}$$

Therefore:

$$I \cong \frac{N_e}{2N_e - N_o} \frac{\Omega(0)}{4\pi} \frac{A(0)}{A(L)} \frac{1}{\tau} \frac{1}{\sqrt{\ln G_o}} \left[2\sqrt{\frac{\ln 2}{\pi}} \cong 1\right] \tag{13}$$

For the oscillator alone, during the pump phase

$$\frac{N_e}{2N_e - N_o} \cong 1.2$$

$$\frac{\Omega(0)}{4\pi} = 2.1 \times 10^{-5} \qquad \text{(8-inch rod, 5 inches from reflector, } n = 1.756, \alpha = 0.0184\text{)}$$

And

$$\frac{A(0)}{A(L)} \cong \frac{1}{10}$$

$$G_o = 10^4 \qquad \text{(rod doubled effectively)}$$

$$\sqrt{\ln G_o} \cong 3.0$$

Thus

$$I \cong \frac{0.84 \times 10^{-2}}{\tau}$$

So the superfluorescent reduction of the lifetime is negligible in the oscillator during pumping.

The combination of oscillator plus amplifier, case 2, has a dominant superfluorescent path of 1 - 2 - 3 - 2 - 1 - 4 - 5 - 4 - 6 - 7 - 9 - 10 - 11. The total gain in the sequence is about 70 db.

The solid angle factor is:

$$\frac{\Omega(0)}{4\pi} = 5.0 \times 10^{-7} \qquad \text{(taking } 5 \times 10^{-3} \text{ beam divergence external to the oscillator rod and } n = 1.765)$$

So

$$I \cong \frac{1}{\tau}(1.2)(5 \times 10^{-7})(\frac{1}{10})\frac{10^7}{4}$$

$$\cong \frac{1}{\tau}(1.5)$$

which is again negligible. Mode selection would improve it even more.